

# Synthesis, Pharmacological and Biophysical Characterization, and Membrane-Interaction QSAR Analysis of Cationic Amphiphilic Model Compounds<sup>‡</sup>

Christian D. P. Klein,<sup>§</sup> Martin Klingmüller,<sup>‡</sup> Christiane Schellinski,<sup>†</sup> Silke Landmann,<sup>†</sup> Stefanie Hauschild,<sup>†</sup> Dieter Heber,<sup>‡</sup> Klaus Mohr,<sup>†</sup> and A. J. Hopfinger<sup>\*,§</sup>

Laboratory of Molecular Modeling and Design, M/C 781, College of Pharmacy, University of Illinois at Chicago, 833 South Wood Street, Chicago, Illinois 60612-7231, Department of Pharmaceutical Chemistry, Pharmaceutical Institute, University of Kiel, Gutenbergstrasse 76, D-24118 Kiel, Germany, and Department of Pharmacology and Toxicology, Pharmaceutical Institute, University of Bonn, An der Immenburg 4, D-53121 Bonn, Germany

Received December 10, 1998

Cationic amphiphilic drugs have a propensity to interact with biological interphases. This study was designed to gain more insight into the molecular properties of catamphiphilic drugs which govern this type of interaction. A series of phenylpropylamine model compounds were synthesized in which modifications were incorporated at the aromatic part of the molecule. The replacement of  $^{45}\text{Ca}^{2+}$  from phosphatidylserine monolayers served to monitor drug binding to the phospholipid. The influence on the phase-transition temperature of liposomes of dipalmitoylphosphatidic acid was measured to assess the perturbing action of the drugs on the structural organization of phospholipid assemblies. The antiarrhythmic activity of the compounds was determined in Langendorff preparations of guinea pig hearts to assess the membrane-stabilizing action. Quantitative structure–activity relationship (QSAR) models for these endpoints were developed using both intra- and intermolecular QSAR descriptors. Intermolecular membrane-interaction descriptors were derived from molecular dynamics simulations of the compounds in a model phospholipid monolayer. QSAR models were derived for all endpoints using partial least-squares regression (PLS) and a genetic algorithm tool, the genetic function approximation (GFA). Membrane-interaction descriptors appear to be of a particular importance in explaining the influence of the compounds on the phase-transition temperature of DPPA liposomes, while the other endpoints can be adequately modeled by intramolecular descriptors. The calcium-displacing activity at phosphatidylserine monolayers is governed by the electrostatic properties of the compounds. Measures of lipophilicity and molecular size are of particular importance for antiarrhythmic activity. Possible improvements to both the molecular modeling and the applied computational protocol of membrane-solute systems are identified and discussed.

## Introduction

Drugs from a wide variety of pharmacological groups are cationic amphiphilic in nature, such as antiarrhythmics, local anesthetics, antimalarials,  $\beta$ -blockers, and tricyclic antidepressants.<sup>1</sup> The drugs often contain, in close proximity, a lipophilic aromatic ring system and a side chain with a nitrogen protonized at physiological pH. The drugs are prone to interact with membrane phospholipids: the cationic nitrogen is attracted to the negatively charged phosphate of the phospholipid head-

group, and the aromatic ring system is directed toward the hydrophobic interior of the phospholipid layer. The cationic amphiphilic nature may have impact on drug pharmacokinetics and pharmacodynamics.<sup>2</sup>

Many efforts have been made to understand the molecular principles of drug–phospholipid interaction on the molecular level. However, a drawback of applying selected therapeutics as test compounds is their heterogeneity in molecular structure and physicochemical properties. Only very few structure–activity studies for explicit membrane-interaction endpoints have been reported to date.<sup>3</sup> A possible reason for this situation may be the lack of appropriate training datasets. The goal of this study was to synthesize, test, and characterize a set of cationic amphiphilic model compounds (Table 1) and analyze their membrane-interaction behavior in terms of quantitative structure–activity relationship (QSAR) models. In this series of phenylpropylamine derivatives the structure of the aromatic part is the variable parameter while the side chain is kept constant. With a propyl linker between the aromatic ring and the nitrogen, its alkaline character is relatively independent of the aromatic variations.

\* Corresponding author. Phone: (312) 996-4816. Fax: (312) 413-3479. E-mail: hopfingr@uic.edu.

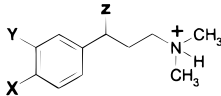
<sup>§</sup> University of Illinois at Chicago.

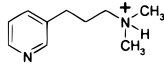
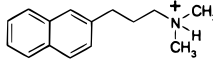
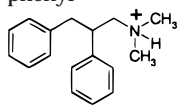
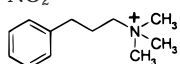
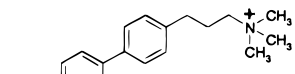
<sup>‡</sup> University of Kiel.

<sup>†</sup> University of Bonn.

<sup>‡</sup> Abbreviations: CPISA, charged partial surface area; DMPC, dimyristoylphosphatidylcholine; DPPA, dipalmitoylphosphatidic acid; DPPC, dipalmitoylphosphatidylcholine; DPPG, dipalmitoylphosphatidylglycerol; DSC, differential scanning calorimetry; ESR, electron spin resonance; GFA, genetic function approximation; HPLC, high-performance liquid chromatography; LOF, lack of fit; MDR, multiple drug resistance; MDS, molecular dynamics simulation; NMR, nuclear magnetic resonance; PLS, partial least-squares (regression); QSAR, quantitative structure–activity relationship; QSPR, quantitative structure–property relationship; TES, *N*-tris(hydroxymethyl)methyl-2-aminoethanesulfonic acid;  $T_t$ , phase-transition temperature.

Table 1. Synthesis of the Compounds



compd	X	Y	Z	method	yield (%)	empirical formula <sup>a</sup>	mp (°C)
1	Cl	H	H	A	90	C <sub>11</sub> H <sub>17</sub> Cl <sub>2</sub> N	155
2	Br	H	H	B	95	C <sub>11</sub> H <sub>17</sub> BrClN	139
3	HO	H	H	A	74	C <sub>11</sub> H <sub>18</sub> ClNO	142–144
4				B	93	C <sub>10</sub> H <sub>18</sub> Cl <sub>2</sub> N <sub>2</sub> O <sub>8</sub>	160 <sup>b</sup>
5	phenyl	H	H	A	74	C <sub>17</sub> H <sub>22</sub> ClN	191
6	H	H	H	B	82	C <sub>11</sub> H <sub>18</sub> ClN	144
7	Me	H	H	B	55	C <sub>12</sub> H <sub>20</sub> ClN	174
8	Et	H	H	B	86	C <sub>13</sub> H <sub>22</sub> ClN	178
9	<i>n</i> -Pr	H	H	B	41	C <sub>14</sub> H <sub>24</sub> ClN	198
10	<i>i</i> -Pr	H	H	B	11 <sup>d</sup>	C <sub>14</sub> H <sub>24</sub> ClN	196
11	<i>t</i> -Bu	H	H	B	50	C <sub>15</sub> H <sub>26</sub> ClN	183
12	MeO	H	H	B	85	C <sub>12</sub> H <sub>20</sub> ClNO	158
13	4-Cl-phenyl	H	H	B	83	C <sub>17</sub> H <sub>21</sub> Cl <sub>2</sub> N	197
14	4-MeO-phenyl	H	H	B	42	C <sub>18</sub> H <sub>24</sub> ClNO	231
15	4-EtO-phenyl	H	H	B	92	C <sub>19</sub> H <sub>26</sub> ClNO	239
16				B	68	C <sub>15</sub> H <sub>20</sub> ClN	167
17	MeO	Cl	H	B	87	C <sub>12</sub> H <sub>19</sub> Cl <sub>2</sub> NO	189
18	H	H	phenyl	C	90	C <sub>17</sub> H <sub>22</sub> ClN	165
19	phenyl	H	phenyl	C	89	C <sub>23</sub> H <sub>26</sub> ClN	167–168
20				B	86	C <sub>17</sub> H <sub>22</sub> ClN	167–169
21	NO <sub>2</sub>	H	H	B	28	C <sub>11</sub> H <sub>17</sub> ClN <sub>2</sub> O <sub>2</sub>	154
22				B	88	C <sub>12</sub> H <sub>20</sub> NJ	175 <sup>c</sup>
23	4-HO-phenyl	H	H	B	95	C <sub>17</sub> H <sub>22</sub> ClNO	220–221
24	HO	Cl	H	B	85	C <sub>11</sub> H <sub>17</sub> Cl <sub>2</sub> NO	189
25				B	90	C <sub>19</sub> H <sub>26</sub> NJO	165 <sup>c</sup>
26	NH <sub>2</sub>	H	H	B	80	C <sub>11</sub> H <sub>20</sub> Cl <sub>2</sub> N <sub>2</sub>	250 dec

<sup>a</sup> Analyses for C, H, and N are within  $\pm 0.4\%$  of the theoretical value. All compounds were isolated as hydrochlorides except **4**, **22**, and **25**. <sup>b</sup>Anion = diperchlorate. <sup>c</sup>Anion = iodide. <sup>d</sup>With regard to 4-*n*-propylacetophenone (see Experimental Section).

## Methods

**General Considerations.** The test compounds were studied in three model systems. The inhibition of <sup>45</sup>Ca<sup>2+</sup> adsorption to phosphatidylserine monolayers indicates the interaction of the compounds with the phospholipid surface charge and probably reflects drug binding affinity to the phospholipid.<sup>1,4,5</sup> The drug-induced depression of the transition temperature of dipalmitoylphosphatidic acid (DPPA) liposomes, measured by differential scanning calorimetry, indicates structural perturbation of the phospholipid bilayer. DPPA was chosen because catamphiphilic drugs induce, in this phospholipid, in addition to the control transition, a second, clearly separate signal, the temperature of which is independent of the amount of drug added.<sup>6</sup> The extent to which the transition temperature is reduced has been suggested to reflect the depth of drug penetration into the hydrophobic core of the phospholipid bilayer.<sup>5</sup> The drug-induced elevation of the threshold of alternating current to elicit arrhythmia in isolated, spontaneously beating guinea pig hearts was measured

to assess the membrane-stabilizing potency of the test compounds in an excitable tissue.<sup>1</sup>

The trial descriptors of a QSAR analysis are normally computed from the chemical structures of the molecules composing the training set from which the QSAR is to be constructed. However, there is no reason that the estimation of QSAR descriptors need be restricted to the *intramolecular* properties of a molecule. For example, if the geometry of the receptor to which the training set molecules bind is available, then *intermolecular* ligand–receptor properties can be computed and used as trial QSAR descriptors along with the *intramolecular* descriptors. The information inherent to the ligand–receptor descriptors should allow the construction of a better QSAR model than if this information is neglected or not available. In the study reported in this paper, a membrane model of a phospholipid monolayer has been assumed to be a *general receptor* for the set of cationic amphiphilic compounds studied as antiarrhythmic drug candidates.

The impetus to explore *intermolecular* membrane-interaction descriptors as trial QSAR descriptors is

**Table 2.** Physicochemical Properties, Antiarrhythmic Activity, and Biophysical Properties for the Dataset

compd	log $P_a$	$pK_a^b$	log AC <sub>50</sub> <sup>d</sup> ( $\mu$ M)	$T_i^e$ (K)	log IC <sub>50</sub> <sup>f</sup> ( $\mu$ M)
<b>1</b>	2.21	10.59	<u>4.31</u>	<u>302</u>	<u>3.85</u>
<b>2</b>	2.37	10.62	x	x	x
<b>3</b>	0.35	x	<u>3.29</u>	<u>314</u>	<u>2.72</u>
<b>4</b>	0.57	10.68, 7.15	vl	x	<u>3.60</u>
<b>5</b>	2.99	9.88	<u>4.80</u>	<u>285</u>	<u>5.40</u>
<b>6</b>	1.50	10.96	<u>3.55</u>	<u>308</u>	<u>3.00</u>
<b>7</b>	2.00	10.84	<u>4.02</u>	<u>303</u>	x
<b>8</b>	2.45	10.63	<u>3.94</u>	<u>300</u>	x
<b>9</b>	2.89	10.54	<u>4.85</u>	<u>295</u>	x
<b>10</b>	2.75	10.49	<u>4.22</u>	<u>299</u>	x
<b>11</b>	2.96	10.03	<u>4.52</u>	<u>297</u>	<u>5.40</u>
<b>12</b>	1.48	10.91	<u>3.62</u>	x	x
<b>13</b>	3.45	9.96	<u>5.70</u>	x	x
<b>14</b>	2.95	9.85	<u>4.96</u>	<u>296</u>	<u>5.40</u>
<b>15</b>	3.30	9.82	<u>4.80</u>	x	x
<b>16</b>	2.62	10.27	<u>4.52</u>	<u>297</u>	<u>4.35</u>
<b>17</b>	1.92	10.76	<u>4.44</u>	x	x
<b>18</b>	2.76	10.00	<u>4.37</u>	<u>308</u>	<u>4.85</u>
<b>19</b>	3.36	9.85	x	<u>294</u>	x
<b>20</b>	2.59	9.93	4.13	309	x
<b>21</b>	1.50	10.74	vl	<u>307</u>	<u>4.15</u>
<b>22</b>	0.44	x	vl	<u>307</u>	<u>3.40</u>
<b>23</b>	2.10	9.32	<u>4.43</u>	<u>349</u>	<u>4.40</u>
<b>24</b>	0.97	x	<u>3.82</u>	<u>294</u>	x
<b>25</b>	2.17	x	vl	x	x
<b>26</b>	0.12	10.87, 7.34	<u>3.00</u>	x	x

<sup>a</sup> Determined by RP-HPLC. <sup>b</sup> Measured by aqueous titration of hydrochlorides. <sup>c</sup> Calculated, MOPAC 6.0.<sup>26</sup> <sup>d</sup> Concentration to elevate the threshold of alternating current to induce arrhythmia in isolated guinea pig hearts by 50%. <sup>e</sup> Drug-induced phase-transition temperature of DPPA liposomes/drug mixture. <sup>f</sup> Drug concentration at which Ca<sup>2+</sup> binding to phosphatidylserine monolayers is reduced to 50% of control value. x, not measured; vl, very low activity, could not be measured accurately. Underlined values were included in the QSAR/QSPR analyses of the corresponding property endpoint.

because in an earlier study using intramolecular descriptors,<sup>7</sup> it was not possible to build reliable QSAR and QSPR models for the drug effects on <sup>45</sup>Ca<sup>2+</sup> binding and the phase-transition temperature. This failure can be attributed to the fact that membranes do not offer spatially well-defined binding sites, and a classical, intramolecular QSAR approach may be inappropriate. Thus, we developed an intermolecular modeling approach, based upon molecular dynamics simulations (MDS), of the compounds in a phospholipid environment, the results of which will be reported here. Numerous MDS studies of phospholipid membranes have been reported during the past few years, and in some cases, the behavior of solutes in a model membrane was studied.<sup>8,9</sup> For a recent comprehensive review of membrane MDS studies, see Tieleman et al.<sup>10</sup> To our knowledge, only qualitative or, at best, semiquantitative information on solute–membrane interactions, and the resulting changes in membrane properties, has been derived from MDSs of membranes. One of the main reasons for this situation is the computational overhead of performing membrane MDSs. The methodology used in this approach incorporates a simplified membrane system, to keep the computational cost at a reasonable level. Classical intramolecular solute descriptors and grid cell occupancy descriptors<sup>11</sup> were also included in the QSAR/QSPR model-building process.

The chemical structures and the synthetic schemes for the compounds are given in Table 1; biophysical properties are listed in Table 2. Compounds **16** and **17**

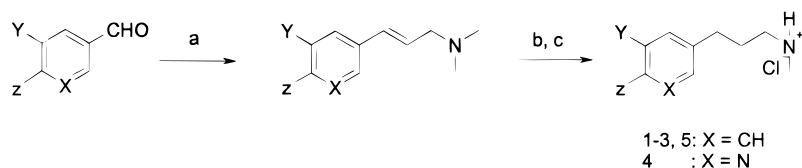
are chiral, and DSC measurements were performed with the racemate. For that reason, and in order to allow for an external validation of the QSAR models, these two analogues were excluded from the training data set. Compound **18** has a significantly different influence on the phase behavior of DPPA liposomes than the other analogues. Compound **18** raises the phase-transition temperature. Therefore, it was judged reasonable to exclude this compound from the training data set constructed for this investigation.

The given dataset appears to be particularly suitable for performing *membrane-interaction QSAR analysis*, as we term this modeling method, because there is minimal uncertainty about the orientation of these compounds within the phospholipid membrane. The cationic amino group is presumably anchored near the phospholipid headgroup region, or the membrane–water interphase, while the aromatic hydrocarbon part is located within the core region of the membrane. Experimental evidence for this arrangement was found by Kuroda and Fujiwara,<sup>12</sup> who studied the interactions of cationic amphiphilic drugs, such as lidocaine, with phosphatidylcholine liposomes using H1-NOE NMR spectroscopy.

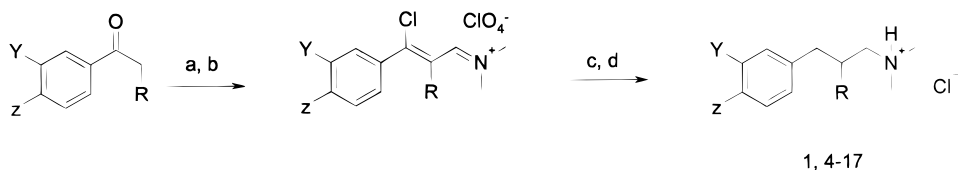
The phospholipid dipalmitoylphosphatidylcholine (DPPC) was used for all MDSs in this study. This choice of phospholipid might, at first glance, surprise, since the DSC measurements were made for DPPA liposomes. However, several considerations led to the belief that DPPC membrane models are, nevertheless, reasonable and lead to valid results. First, most of the published membrane MDSs have been done with either DPPC or, as in our group, dimyristoylphosphatidylcholine (DMPC). Thus far, no MDS study of phosphatidic acid (PA) membranes has come to our attention. The lack of use of PA in membrane modeling may be due to the difficulties in assigning proper ionization states and counterions to the anionic PA headgroups. Second, Hanpft and Mohr,<sup>6</sup> when examining the influence of several cationic amphiphilic compounds on the phase-transition behavior of different phospholipids, found that the transition temperatures of the drug-containing phospholipid domains were practically independent of the phospholipid headgroup in DPPA, DPPC, and dipalmitoylphosphatidylglycerol (DPPG). It was concluded that the intercalation of cationic amphiphilic substances quenches the specific influence of the phospholipid's headgroup on the phase-transition behavior. To check the validity of this approach, measurements were made for selected test compounds in DPPC liposomes. The measured drug-induced transition temperatures favorably corresponded with the predicted values.

**Chemistry.** Several synthetic routes for the preparation of the *N,N*-dimethyl-3-phenylpropylamine (**6**) and substituted derivatives have been reported,<sup>13–17</sup> but these procedures often involve too laborious steps. In this series of model compounds **1–26** the synthesis of ketone Mannich bases and subsequent hydrogenation of their oxo function<sup>16,18</sup> gave unsatisfactory results. Therefore, more convenient methods were developed using the Wittig and Vilsmeier reaction as key steps followed by catalytic hydrogenation of the unsaturated side chain.

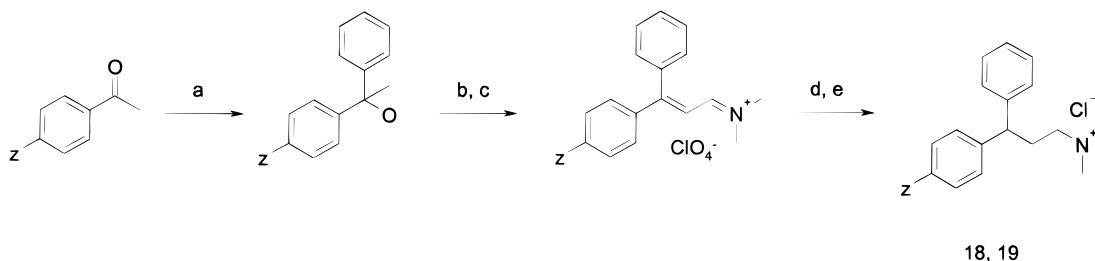
The first strategy developed for the preparation of our model compounds was based on their structural simi-

Scheme 1<sup>a</sup>

<sup>a</sup> (a) *N,N*-Dimethylaminoethylphosphonium bromide/butyllithium; (b) Pd-C/H<sub>2</sub>; (c) HCl.

Scheme 2<sup>a</sup>

<sup>a</sup> (a) DMF/POCl<sub>3</sub>; (b) HClO<sub>4</sub>; (c) Pd-C/H<sub>2</sub>; (d) HCl. R = H or Ar.

Scheme 3<sup>a</sup>

<sup>a</sup> (a) PhMgBr; (b) DMF/POCl<sub>3</sub>; (c) HClO<sub>4</sub>; (d) Pd-C/H<sub>2</sub>; (e) HCl.

larity with cinnamylamine derivatives (Scheme 1) prepared by the method of Marxer and Leutert.<sup>19</sup> It prompted us to treat appropriate para-substituted benzaldehydes with *N,N*-dimethylaminoethylphosphonium bromide and butyllithium as a strong base to give the corresponding allylamines. Hydrogenation of the side chain in the presence of palladium-on-carbon followed by reaction with hydrochloric acid produced the amine hydrochlorides **1–5**. As expected, the phenolic amine **3** was directly formed by hydrogenation of the *p*-benzyloxycinnamylamine derivative involving cleavage of the benzyloxyphenyl ether moiety.

Since this procedure generally proved to be rather complicated and, furthermore, specially substituted carbaldehydes were not as accessible as the corresponding acetophenones, another route was performed according to the method depicted in Scheme 2. Vilsmeier reaction of the appropriate acetophenones was accomplished using phosphorus oxychloride in *N,N*-dimethylformamide to give 3-chloro-2-propeniminium salts isolated as perchlorates<sup>20,21</sup> except for the iminium salt to be required for the preparation of **9** (see Experimental Section). In this procedure, the carbonyl function is invariably substituted by the chlorine atom via the corresponding enol group. The 3-chloro-2-propeniminium salts were catalytically hydrogenated using palladium-on-carbon, and the resulting amines converted to the hydrochlorides **1** and **4–17** in the usual manner. All double bonds were reduced, accompanied by hydrogenolytic cleavage of the chlorine atom. Starting from benzyl phenyl ketone, this procedure could also be successfully applied for the preparation of the 2,3-diphenylpropylamine (**20**). The method proved not to be suitable for the preparation of the nitramine **21** as well as the phenolic amines **3**, **23**, and **24** which required

subsequent heating of **12**, **14**, and **17** in hydrobromic acid. The resulting hydrobromides were converted to the corresponding hydrochlorides. Furthermore, it was found that the nitro group could be conveniently introduced in the para-position of the aromatic ring by simple nitration of **6** to yield the nitrobenzene derivative **21**, which was catalytically hydrogenated using palladium-on-carbon to give para-substituted aniline **26**. Finally, some trialkylpropylammonium salts were prepared by methylation using methyl iodide and subsequent anion exchange to give the hydrochlorides **22** and **25**.

*N,N*-Dimethylamino-3,3-diphenylpropylamine hydrochlorides **18**<sup>22</sup> and **19** were prepared by treatment of the appropriate acetophenone with phenylmagnesium bromide, subsequent Vilsmeier formylation of the 1,1-diphenylethanol, and catalytic hydrogenation of the resulting 3,3-diphenyl-2-propeniminium salt (Scheme 3).

Partition coefficients were determined by HPLC on an RP18 column and different methanol/water mobile phases. The capacity factors were extrapolated to a 100% aqueous medium. The system was calibrated using different aromatic hydrocarbons of known lipophilicity. p*K*<sub>a</sub> values were determined by aqueous titration of the hydrochlorides.

**Pharmacology. 1. <sup>45</sup>Ca<sup>2+</sup> Binding to Monolayers of Phosphatidylserine.** A detailed description of the experimental procedure was given before.<sup>1</sup> In short, a Teflon planchette of 4.5-cm diameter was filled with 5 mL of buffer (0.01 mM CaCl<sub>2</sub> supplemented with trace amounts of <sup>45</sup>CaCl<sub>2</sub>, 5 mM NaCl, 2 mM TES, 2 mM histidine; pH 7.5). Radioactivity was detected by a Geiger-Müller counting tube (Friesseke & Hoepfner, Erlangen, Germany) positioned above the Teflon dish; 3 nmol of phosphatidylserine (from bovine brain; purity 98–99%, Sigma Chemical) dissolved in 1 μL of chloro-



form was carefully applied to the surface of the buffer to form a phospholipid monolayer. Adsorption of  $^{45}\text{Ca}^{2+}$  to the phospholipid was indicated by a 2-fold elevation of the counting rate under control conditions. Test compounds were dissolved in the buffer at the appropriate concentrations.

**2. Phase-Transition Temperature of DPPA Liposomes.** As described previously in detail,<sup>6,15</sup> liposomes of dipalmitoyl-*sn*-glycero-3-phosphate monosodium salt (purity 99%, Sigma Chemical) were prepared in a buffer of 14 mM TES, 14 mM histidine, pH 6, containing appropriate amounts of test compound; 10  $\mu\text{L}$  of the suspension was placed into an aluminum capsule (Perkin-Elmer, Ueberlingen, Germany) which was placed in a differential scanning calorimetry equipment (DSC-2C/Intracooler II, Perkin-Elmer). The sample was heated from 12 to 72 °C at a rate of 5 °C/min. The temperature of the upward deflection of the transition signal was used to indicate the phase-transition temperature which occurred under control conditions at about 65 °C.

**3. Excitability of Isolated Beating Guinea Pig Hearts.** The procedure to induce arrhythmia by alternating current in guinea pig heart Langendorff preparations was described previously.<sup>1</sup> The hearts were perfused through the coronary vasculature with Tyrode's solution modified according to von Muralt (137 mM NaCl, 2.7 mM KCl, 1.8 mM  $\text{CaCl}_2$ , 11.9 mM  $\text{NaHCO}_3$ , 1.1 mM  $\text{MgCl}_2$ , 0.2 mM  $\text{NaH}_2\text{PO}_4$ , 5.5 mM glucose; oxygenated by 95%  $\text{O}_2$ /5%  $\text{CO}_2$ ; pH 7.3; 35 °C). Contractions were recorded via a fine hook fixed to the apex of the heart. To determine the threshold current for arrhythmia, a 50-Hz alternating current of increasing intensity was applied through two fine flexible brushes (diameter 5 mm) soaked with Tyrode's solution and attached in opposite positions to the ventricular myocardium. Test compounds were dissolved in the perfusion medium and applied over a period of 30 min before measurement of the threshold current for arrhythmia. Concentrations were increased in cumulative fashion.

**Membrane-Interaction QSAR Analysis. 1. Building the Molecules and the Simulation System.** All compounds were built using the building tool and library fragments of Chemlab-II.<sup>23</sup> The dimethylaminopropyl side chains were assigned all-trans conformations. The side chain amino groups are protonated under physiological conditions (see  $\text{p}K_a$  values, Table 2). Accordingly, the compounds were built as monocations. DPPC was initially built in HyperChem,<sup>24</sup> using available crystal structure data for DMPC.<sup>25</sup> Calculations at the semiempirical MO level were carried out on the solute molecules and DPPC to assign partial atomic charges and to further optimize molecular geometry. The AM1 Hamiltonian, implemented in the MOPAC 6.0<sup>26</sup> program, was employed.

An assembly of 4\*4\*1 DPPC molecules, resembling a monolayer, was used as a starting structure for an equilibration MDS. The cell parameters for an individual phospholipid molecule were 8\*8\*32 Å,  $\gamma = 97.4$ . These parameters result in an average surface area per phospholipid of 64 Å<sup>2</sup>, which is close to the reported value of about 62 Å<sup>2</sup> for the fully hydrated fluid lamellar (L $\alpha$ ) phase of DPPC.<sup>27</sup> As in the previous studies performed by our group,<sup>9,28,29</sup> an extended MM2 force

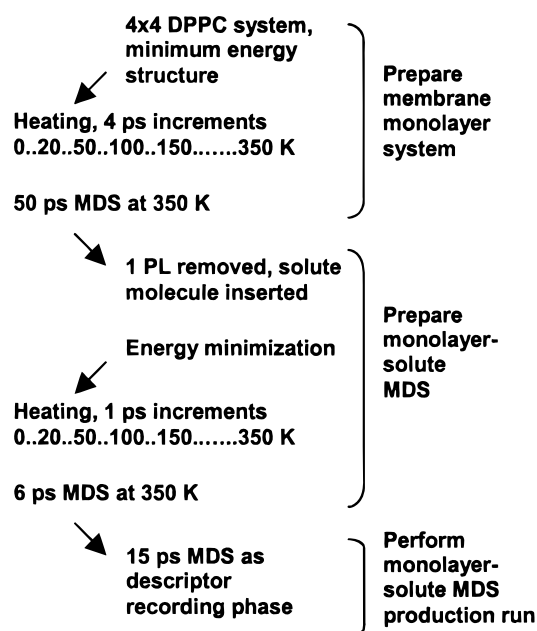


**Figure 1.** MDS sampling protocol for the membrane-solute interaction modeling.

field and the molecular dynamics modeling program MOLSIM<sup>30</sup> were employed for all MDSs. The computational protocol for the MDS is outlined in Figure 1. A time step of 0.001 ps was used in all MDSs. Trajectory data, i.e., atomic positions and system energies, were recorded every 100 steps. Two-dimensional (the "plane" of the monolayer) periodic boundary conditions were applied. Temperature scaling was accomplished by coupling the system to an external constant-temperature bath.<sup>31</sup>

The model monolayer was first heated to 20 K and then to 50 K and from that point in increments of 50 K to a final temperature of 350 K. At each temperature increment, 4 ps of MDS was carried out to allow for structural relaxation and distribution of kinetic energy throughout the system. When 350 K was reached, 50 ps of MDS was performed in order to equilibrate the system.

One DPPC molecule was removed from the equilibrated monolayer model. The test solute molecule was then inserted into the resulting "hole", its propylamino side chains being oriented toward the "aqueous interface" side of the monolayer and the protonated amino groups located near the phospholipid headgroup region. However, three different monolayer-solute alignments were examined for compounds **1**, **6**, **11**, and **18**, respectively. These compounds were chosen as a subset for extensive alignment analysis because they cover a wide range of influence on  $T_t$ . The four alignments examined are depicted schematically in Figure 2.

To remove unfavorable high-energy van der Waals interactions between solute and phospholipid molecules, the energy of the system was minimized by a series of steepest descent and conjugate gradient minimization steps. The energy convergence criterion was a gradient of less than 0.5 kcal/(Å·mol). Convergence was generally achieved within less than 200 steps.

The monolayer-solute systems were reheated using the same heating schedule as described previously for the monolayers. Equilibration periods were 1 ps/heating

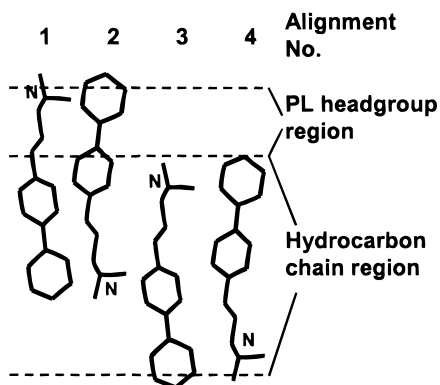


**Figure 2.** Solute alignments explored in the phospholipid matrix. Alignment 1 was used as the starting point for the generation of the membrane–solute interaction descriptors.

**Table 3.** Descriptors Derived from the Membrane-Interaction MDSs

$E_{\text{inter(AVG)}}$	interaction energy between solute and membrane averaged over the MD trajectory (sum of H-bond, electrostatic, and vdW contributions)
$E_{\text{inter(MIN)}}$	interaction energy between solute and membrane at total system minimum potential energy (sum of H-bond, electrostatic, and vdW contributions)
$E_{\text{inter(AVG\_HBD)}}$	$E_{\text{inter(AVG)}}$ for H-bond interactions
$E_{\text{inter(MIN\_HBD)}}$	$E_{\text{inter(MIN)}}$ for H-bond interactions
$E_{\text{inter(AVG\_COU)}}$	$E_{\text{inter(AVG)}}$ for electrostatic interactions
$E_{\text{inter(MIN\_COU)}}$	$E_{\text{inter(MIN)}}$ for electrostatic interactions
$E_{\text{inter(AVG\_VDW)}}$	$E_{\text{inter(AVG)}}$ for van der Waals interactions
$E_{\text{inter(MIN\_VDW)}}$	$E_{\text{inter(MIN)}}$ for van der Waals interactions
$d\rho$	change in membrane density upon uptake of the solute
$dS$	change in membrane entropy upon uptake of a solute molecule
$D$	diffusion coefficient of a solute in the membrane
$\langle d \rangle$	average depth of a solute in the membrane

increment. Production trajectories were recorded over 20-ps MDS runs at 350 K. Membrane–solute interaction descriptors were calculated using the last 15 ps of these runs. For reference purposes, an undisturbed monolayer model, without any phospholipids removed or solutes inserted, was modeled in the same way as the membrane–solute systems.

**2. Calculation of Membrane-Interaction Descriptors.** The membrane–interaction descriptors determined from the production runs are defined in Table 3. Solute–membrane interaction energies were extracted from the intermolecular interaction energy trajectory files. Other membrane–interaction descriptors were calculated as described in the Computational Details section.

**3. Calculation of Intramolecular Descriptors.** Intramolecular solute descriptors were calculated manually, or by means of the molecular modeling package Cerius2, release 3.0.<sup>32</sup> AM1-minimized solute structures were used for the intramolecular descriptor calculations. The compounds were aligned using the side chain nitrogen, the phenyl-C1, and the phenyl-C4 as alignment atoms. All of the intramolecular descriptors considered in QSPR model building are listed in Table 4. The charged partial surface area (CPSA) descriptors of Stanton and Jurs<sup>33</sup> are not individually reported.

**4. Construction of QSAR/QSPR Models.** QSPR models were built using the program Wolf 6.2.<sup>34</sup> Wolf

**Table 4.** Intramolecular Solute Descriptors

descriptor	source
log $P$ (logarithm of the partition coefficient)	<i>a</i>
sum of atomic polarizabilities	<i>b</i>
superdelocalizability	<i>b</i>
HOMO	<i>c</i>
LUMO	<i>c</i>
dipole moment	<i>c</i>
heat of formation	<i>c</i>
Jurs–Stanton CPSA (charged partial surface area) descriptors	<i>b</i>
radius of gyration	<i>b</i>
van der Waals surface area	<i>b</i>
molecular volume	<i>b</i>
density	<i>b</i>
no. of rotatable bonds	<i>b</i>
no. of hydrogen bond acceptors	<i>d</i>
no. of hydrogen bond donors	<i>d</i>
molecular weight	<i>c</i>
calculated octanol/water partition coefficient	<i>b</i>
molar refractivity	<i>b</i>
desolvation free energy for water	<i>b</i>
desolvation free energy for octanol	<i>b</i>

<sup>a</sup> Experimental value.<sup>10</sup> <sup>b</sup> Computed.<sup>30</sup> <sup>c</sup> Calculated, MOPAC 6.22 <sup>d</sup> Determined manually.

employs partial least-squares (PLS) regression,<sup>35</sup> combined with a method based on genetic algorithms, the genetic function approximation (GFA),<sup>36</sup> which is used for model building. Friedman's lack-of-fit (LOF) measure is used as the ranking/score function during model evolution.<sup>37</sup> The LOF contains a penalty term for independent variable model size (the smoothing factor) and is the default ranking score of the Wolf program. All descriptors were mean-scaled and centered. An initial random population of 300 models was used. The 20 best-scoring models of the final GFA populations were cross-validated, using the leave-one-out ( $n$ -fold) cross-validation technique. GFA crossover parameters were varied for each endpoint until a GFA model population of optimal statistic quality, defined in terms of the average cross-validated  $r^2$  of the 20 best models, was obtained.

Attempts were made to build QSPR models with linear and with linear and quadratic basis set functions (terms). Purely linear models were statistically less significant than combined quadratic/linear models. In general, however, the same descriptors were of major significance in both the linear and quadratic/linear model populations. Therefore, model populations were initialized with the same creation probability for both linear and quadratic basis functions.

The two chiral compounds **19** and **20** were not included in any of the training datasets, because the pharmacological and biophysical testing had been done with the racemates. However, predictions were made for the stereoisomers of both compounds. Compound **23** elevates the phase-transition temperature of DPPA. This behavior was not observed for any other compound in the dataset, and it was thus judged reasonable to exclude this compound from the training dataset for phase-transition temperature.

## Results and Discussion

**Pharmacology.** The test compounds inhibit, in a concentration-dependent manner, the binding of  $^{45}\text{Ca}^{2+}$  to phosphatidylserine monolayers as has been previously illustrated for cationic amphiphilic therapeutics.<sup>1</sup>

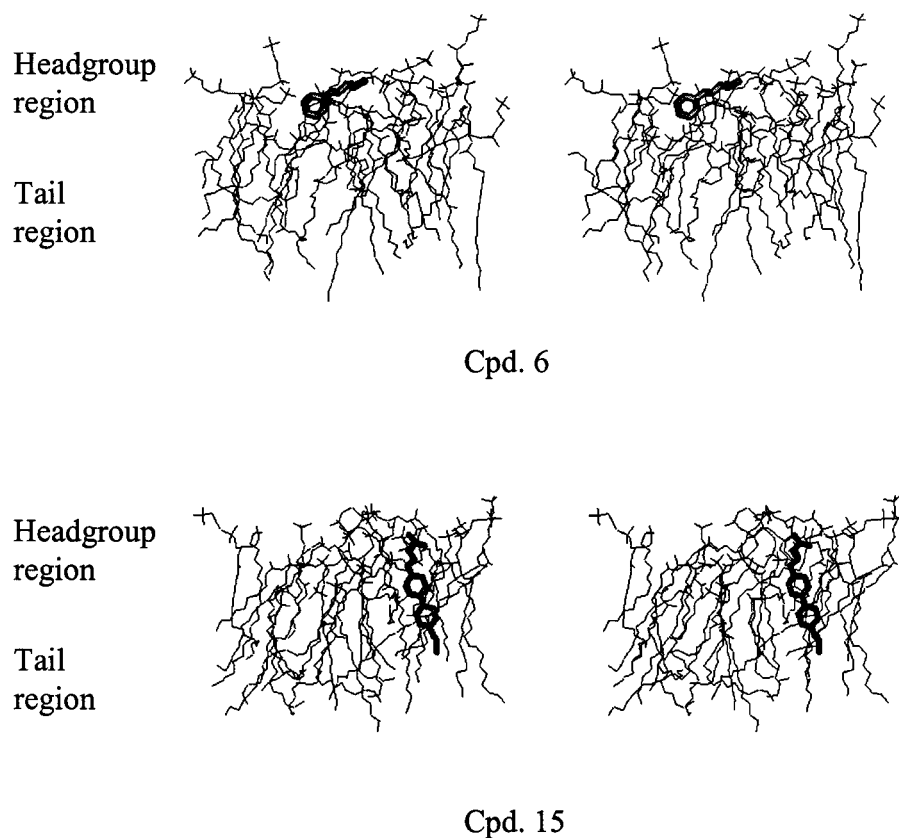


**Figure 3.** Stereographic representations of the lowest potential energy states from the MDS of compounds **6** and **15** interacting with the model DPPC monolayer. Compound **6**, the unsubstituted "parent" compound of the dataset, is preferably located within the headgroup region, while compound **15** inserts into the DPPC monolayer and aligns itself parallel to the hydrocarbon chains.

The measure of potency is the concentration of the test compound at which  $^{45}\text{Ca}^{2+}$  binding is reduced to 50% of the control value, i.e.,  $^{45}\text{Ca}^{2+}$  adsorption to the phospholipid measured in the absence of test compound ( $\text{IC}_{50}$  values, cf. Table 2).

The phase transition of DPPA liposomes is affected by the test compounds as has been illustrated previously for cationic amphiphilic therapeutics<sup>1,6</sup> and for the test compounds **5**, **6**, and **18**.<sup>5</sup> The temperature of the drug-induced signal is specific for a given test compound (Table 2).

The threshold current for arrhythmia increases in the presence of the test compounds in a concentration-dependent fashion as has been previously illustrated for cationic amphiphilic therapeutics.<sup>1</sup> The drug concentration at which the threshold current is elevated by 50% over the control value in the absence of test compounds is used as a measure of the membrane-stabilizing potency ( $\text{AC}_{50}$  values, cf. Table 2).<sup>1</sup> The  $\text{AC}_{50}$  to suppress myocardial excitability may be taken to reflect the potency of a drug to block voltage-dependent sodium channels.

**Membrane-Solute MDSs.** A comparison of the MDS trajectories for the different solute arrangements in the phospholipid matrix (cf. Figure 2) indicated the initial alignment 1 to be generally more stable than the other alignments. This finding can be inferred from a visual inspection of the MDS atomic position trajectories by means of the MOLSIM visualization tool, MDMOVIE, as well as from an inspection of the membrane-solute interaction energies and the total system potential energies, which are, for most of the com-

pounds, the lowest (most stable) for alignment 1. The MDS trajectories for alignment 3 generally show movement of the solute toward the phospholipid headgroup region, until a final state, similar to alignment 1, is reached. Both alignments 2 and 4 do not lead to stable positions of the solute in the membrane.

Visual inspection of the MDS trajectories obtained with alignment 1 revealed that the majority of the solutes did not show any pronounced overall movement away from their initial positions. Some compounds, however, did behave differently. Compounds **2**, **11**, and **18** adopt positions which can be described as "parallel" to the monolayer plane. In this alignment, the compounds interact mainly with the headgroup region of the model monolayer and are virtually inserted into it. A similar, but less pronounced, tendency to migrate from the initial alignment position toward the headgroup region can be seen with compounds **6**, **13**, **16**, and **17**. In any case, the major movement starts during the heating process and is finished before the start of the production run. This observation is consistent with the calculated diffusion coefficients for the production runs, which range from  $10^{-10}$  to  $10^{-9}$   $\text{cm}^2/\text{s}$  over the data set. The highest diffusion coefficients are observed for the small compounds, such as **10** and **14**. Large compounds, such as the stereoisomers of compound **16**, experience smaller degrees of mobility, which is reflected by lower computed diffusion coefficients. Graphical representations of the minimum potential energy states sampled over the course of the MDS for compounds **6** and **15**, respectively, are shown in Figure 3.

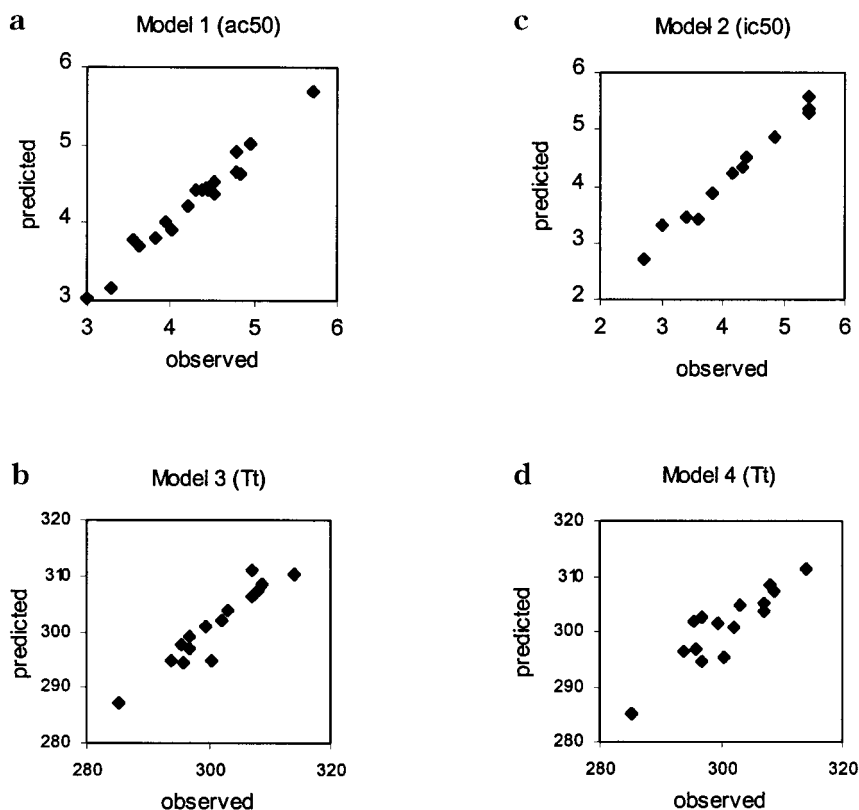


**Figure 4.** Predicted vs observed (a)  $-\log AC_{50}$ , (b)  $-\log IC_{50}$ , (c)  $T_i$ , and (d)  $T_i$  for the QSAR models given by eqs 1–4 in the text.

The average depth of a solute in the membrane, defined as the "depth" descriptor, ranges from 12.5 to 18 Å. These values may seem large, given a monolayer thickness of about 20 Å. However, the distance to the single, closest phospholipid headgroup is always much smaller and amounts to around 6 Å for most of the solutes. Still, it does not seem appropriate to only look at the distance to the closest phospholipid, since the headgroups sometimes undergo a considerable degree of vertical movement. If, instead, the average distance to the five closest headgroups is taken as a measure for solute depth, the idea of a phospholipid headgroup region is retained. Some of the five closest phospholipid phosphorus atoms have relatively large, lateral (parallel to the monolayer plane) distances from the solute, which increases the average distance values. Both the average and minimum membrane–solute interaction energies span a relatively wide range of values. The most stabilizing interactions arise for compound **1**, with  $E_{\text{inter(AVG)}} = -58.9$  kcal/mol, followed by compound **13** and the stereoisomers of compound **16**. Differences in membrane–solute interaction energies as well as other membrane-dependent descriptors are, in most cases, small for pairs of stereoisomers. For example,  $E_{\text{inter(AVG)}}$  is  $-52.0$  kcal/mol for *R*-**16** and  $-56.0$  kcal/mol for *S*-**16**. The entropy of the model membranes shows practically no change after uptake of the solute, and membrane density varies only slightly. This is reasonable for low concentrations (1/15) of solutes in the monolayer.

**QSAR for Antiarrhythmic Activity.** The model population resulting from the GFA run consists of two-, three-, and four-term models, practically all of which are linear. The most often used descriptor is clearly  $\log P$ , which is found in about 60% of all QSAR models.

Surprisingly, it is not incorporated in the best-scoring model:

$$-\log AC_{50} = 2.572 + 7.37*(\text{acp}^*4^* - 2*10^*0) + 0.000378*\text{APol} + 0.07647*\text{F-H}_2\text{O} - 0.072175*\text{WPSA-3} \quad (1)$$

$$\text{LOF} = 0.085, r^2 = 0.97, \text{xv-}r^2 = 0.94, \text{SE} = 0.155, n = 19$$

where LOF, Friedman's lack-of-fit score; xv- $r^2$ , cross-validated  $r^2$ ; SE, standard error; (acp\*4\* - 2\*10\*0), grid cell occupancy descriptor determined by MDS using 4D-QSAR analysis;<sup>7</sup> WPSA-3, surface weighted positive surface area;<sup>33</sup> APol, sum of atomic polarizabilities;<sup>38</sup> F-H<sub>2</sub>O, aqueous desolvation free energy;<sup>39</sup> GFA options, 80 000 crossover operations, smoothing factor = 2.

The fit and predictive quality of this model is equal to the hybrid grid cell/ $\log P$  model reported in ref 7, but it contains only four variables as compared to the five-variable model reported previously. One of the descriptors (WPSA-3) of eq 1 is modestly correlated to  $\log P$  ( $r^2 = 0.73$  for the training set of 19 compounds) and might be regarded as a substitute for this measure. Except for WPSA-3 and the grid cell occupancy descriptor ( $r^2 = 0.69$ ), no substantial cross-correlations among the descriptors of the model can be found. Plots of predicted versus observed  $-\log AC_{50}$  values are shown in Figure 4, part a. An inspection of this plot reveals that there are no major outliers or ranges in  $-\log AC_{50}$  where the QSAR fit is particularly poor.

Equation 1 is consistent with the local anesthetics receptor concept, in that it incorporates a 4D-QSAR grid cell occupancy descriptor<sup>11</sup> as a measure of molecular



geometry. Furthermore, it has long been known<sup>1,40</sup> that lipophilicity is the major factor in determining the antiarrhythmic activity of cationic amphiphilic drugs. This suggests that the spatial requirements of the receptor are comparably unspecific and lipophilic interactions play a major role in the inactivation process.

Compound **20** is chiral, and since the antiarrhythmic activity has been measured for the racemate, it was not included in the training dataset. Predictions for both stereoisomers were made using eq 1. The predicted values are 4.5 and 4.4, respectively. Both of these values are very close to the measured activity of 4.1, and this emphasizes the predictive quality of the QSAR model.

**QSPR for Inhibition of Calcium Ion Binding to PS Monolayers.** The inhibition of calcium ion binding to PS monolayers had been measured for only 12 compounds. QSPR models which are based on such a small dataset will have to be evaluated with particular carefulness. The best QSPR model incorporates three descriptors:

$$-\log IC_{50} = -5.24 + 0.019*TPSA + 0.111*(Dipole-Z - 1.34)^2 + 12.11*RPCG \quad (2)$$

$$LOF = 0.104, r^2 = 0.98, xv-r^2 = 0.79, SE = 0.155, n = 12$$

where LOF, Friedman's lack-of-fit score;  $xv-r^2$ , cross-validated  $r^2$ ; SE, standard error; TPSA, total polar surface area; Dipole- $Z$ , dipole moment in the  $Z$  direction, where  $Z$  is one of Cartesian axes; RPCG, relative positive charge (charge of most positive atom/total positive charge); GFA options, 80 000 crossovers, smoothing factor = 1.5.

The main conclusion that can be made from an inspection of this QSPR model is that the replacement of calcium ions is an electrostatically driven process. All descriptors are positively correlated with potency. Calcium ions and cationic amphiphilic compounds bind to the negatively charged headgroup of phosphatidylserine, which is exposed to the aqueous phase in the assay system. The insertion of the analogues into the phospholipid phase appears to be of minor importance for their activity, since no lipophilicity measure or membrane-interaction descriptor is of major significance in the final QSPR model population. The most often used descriptors are TPSA, RPCG, Dipole- $Z$  (see eq 2), the grid cell occupancy descriptors, and Dipole- $X$  (dipole moment in the  $X$  direction). Plots of predicted versus observed  $-\log IC_{50}$  values are given in Figure 4, part b. The lower and upper ranges in  $-\log IC_{50}$  appear to contain the major lack of fits between the QSPR model and the observed data.

**QSPR for the Depression of  $T_t$  in DPPA Liposomes.** The GFA model-building process (80 000 crossovers, smoothing factor = 1.5) for the  $T_t$  endpoint resulted in a population of two- and three-descriptor models. The most often used descriptors were one of the CPSA descriptors (FPSA-3, a fractional positive surface charge measure), the membrane-solute interaction energy at the total potential energy minimum state of the simulation system, and the radius of gyration of the compounds. The best two- and three-term models are given as eqs 3 and 4 below:

$$T_t = 298.18 - 0.023*(E_{inter(MIN\_VDW)} + 18.68)^2 - 0.105*(PPSA\_3 - 43.198)^2 + 9.070*(ROG - 5.199)^2 \quad (3)$$

$$LOF = 21.55, r^2 = 0.89, xv-r^2 = 0.82, SE = 2.95, n = 15$$

$$T_t = 300.34 - 0.023*(E_{inter(MIN)} + 32.14)^2 + 97060.0*(FPSA\_3 - 0.068)^2 \quad (4)$$

$$LOF = 20.92, r^2 = 0.81, xv-r^2 = 0.68, SE = 3.90, n = 15$$

where LOF, Friedman's lack-of-fit score;  $xv-r^2$ ; cross-validated  $r^2$ ; SE, standard error; ROG, radius of gyration;  $E_{inter(MIN)}$ , PPSA\_3, and FPSA\_3; see text.

Both QSAR models, eqs 3 and 4, include one descriptor derived from the membrane MDS. These intermolecular descriptors are the total and the van der Waals interaction energies between solute and phospholipids at the minimum potential energy state of the simulation system ( $E_{inter(MIN)}$  and  $E_{inter(MIN\_VDW)}$ ). Also, surface charge measures are included in both models. Equation 3, in addition, incorporates another intramolecular term, the radius of gyration of the compounds. Obviously, the intermolecular descriptors, which were derived from the membrane MDS, are of significant value for explaining the influence of the compounds on the DPPA phase-transition temperature.

Although models 3 and 4 incorporate quadratic terms, no real parabolic relationship exists between the descriptors and the considered endpoint. The presence of quadratic terms allows a better fit to the training data set, but no minimum or maximum can actually be seen with the descriptor values in the training set. Plots of predicted versus observed  $T_t$  are given in Figure 4, parts c and d. Equation 4, part d of Figure 4, shows more scatter between predicted and observed  $T_t$  values, particularly in the middle of the  $T_t$  range, than eq 3, part c of Figure 4.

The solute-membrane interaction energy descriptors,  $E_{inter(MIN)}$  and  $E_{inter(MIN\_VDW)}$ , are positively correlated with membrane-transition temperature. This means that a more endergonic interaction of a solute with the membrane will lead to a more pronounced depression of the phase-transition temperature. This observation can be interpreted in the following fashion: Differences in interaction energies, from  $E_{inter(MIN\_VDW)}$ ,  $E_{inter(MIN\_COU)}$ , or  $E_{inter(MIN)}$ , largely originate from differences in the location and alignment of the solute in the membrane. For instance, a solute which is oriented parallel to the alkyl chain, with its hydrophobic moiety inserted between them, will experience a more endergonic interaction with its phospholipid neighbors than a solute that is located between the headgroups on the monolayer surface and has a larger part of its molecular surface exposed to the "aqueous" outside. Therefore, interaction energies, in particular  $E_{inter(MIN\_VDW)}$ , can be regarded as measures of the extent to which a solute interacts with the phospholipid hydrocarbon chains. Compounds that experience a stronger interdigitation between the chains, such as compound **5**, introduce a more pronounced destabilizing effect into this region of the membrane. Thus, these compounds lower the phase-

transition temperature to a larger extent than solutes which do not interdigitate as significantly, such as compound **21**.

The two CPSA descriptors, PPSA-3 and FPSA-3, that appear to be of major significance in the  $T_t$  QSPR models are both measures of positively charged solute molecular surface area. PPSA-3 is defined as the sum of the product of the [solvent-accessible surface area  $\times$  partial charge] for all positively charged atoms of the solute. FPSA-3 is obtained from PPSA-3 by dividing by the total molecular solvent-accessible surface area.<sup>33</sup> Both of these descriptors are positively correlated with transition temperature: i.e., molecules with more negatively charged surfaces induce larger declines in  $T_t$  than molecules with positively charged surfaces. One possible interpretation for the importance of these descriptors in the QSPR models is that these descriptors reflect the influence of the solutes on the electrostatic environment of the membrane-water interphase and the electrostatic stability of the headgroup region in particular. DPPA is the phospholipid used in the experimental studies and possesses anionic headgroups, while DPPC is an effectively neutral molecule. The CPSA descriptors may, in this respect, act as corrections which account for electrostatic differences between these two phospholipids. Another possible explanation can be inferred from the fact that the phospholipid hydrocarbon chains have slightly positively charged surfaces, resulting in a repulsive interaction with solutes also having positive surface charges. The charge repulsions would also lead to less of an insertion of such a solute into the hydrocarbon chain region of the membrane.

The radius of gyration is calculated from the atomic coordinates of a molecule relative to its center of mass and can, therefore, for small molecules, be regarded as an indirect measure of molecular branching and size. This molecular property is often used in biopolymer modeling, particularly to describe the folding state of proteins and other biomolecules.<sup>39</sup> For the solutes considered in this study, a large radius of gyration is associated with a large depression in  $T_t$ . Compounds in the training set with large radii of gyration are larger and more elongated than other analogues. Therefore, if an anchoring of the solute amine group to the phospholipid headgroup region is assumed, compounds with large radii of gyration reach further into the hydrocarbon chain region than other analogues. This interpretation is similar to the one given for the membrane-interaction energy descriptors,  $E_{\text{inter(MIN)}}$  and  $E_{\text{inter(MIN\_VDW)}}$ . However, the membrane-interaction descriptors are only weakly correlated to the radius of gyration.

The radius of gyration might also provide corrections and/or enhancements to data generated in the MDSs. Such corrections and enhancements may be needed because by performing only one MDS per compound, metastable conformations and alignments of the solutes in the membrane cannot always be identified. Thus, descriptors derived from the simulations are necessarily biased. For example, the aromatic moiety of compound **14** does not penetrate as far into the monolayer as is the case with compound **5**. Consequently, the membrane-solute van der Waals interaction energy for compound **14** is much lower than for compound **5**. This

**Table 5.** Predicted and Observed Transition Temperatures (K) for Solutes That Were Not Included in the Training Set

compd	$T_t$ (pred) model 3	$T_t$ (pred) model 4	$T_t$ (obsd)
<i>R-19</i>	310	292	294 <sup>a</sup>
<i>S-19</i>	306	292	294 <sup>a</sup>
<i>R-20</i>	320	323	309 <sup>a</sup>
<i>S-20</i>	325	322	309 <sup>a</sup>
<b>23</b>	314	299	349

<sup>a</sup> Measured for the racemate.

behavior might be a real phenomenon, arising from interactions of the solute methoxyl group with the phospholipid headgroups. However, a random effect, introduced by insufficient sampling of thermodynamic states, seems more likely to be the case. Future development on the membrane-interaction QSAR/QSPR methodology will have to take the possibility of insufficient sampling into consideration, and techniques to overcome this limitation will have to be explored. One obvious improvement is to extend the sampling period, but due to the computational overhead of MDSs on large systems, this seems a rather costly approach. A more economic approach might be to run multiple, short simulations on systems with slightly different initial states, i.e., modified molecular positions and initial velocities.

How well do the membrane-interaction QSPR models predict the influence of compounds **19**, **20**, and **23**, which were not included in the training set, on the phase-transition temperature? The predictions from models 3 and 4 are given in Table 5. These are the best two QSPR models from the two distinct families of QSPR models generated in the model optimization process.

Predicted values for the stereoisomers of **19** and **20** do not differ substantially, using either QSPR model. Comparing predicted and observed values, it is found that both models give the correct relative ranking of  $T_t$ : i.e., the  $T_t$  for compound **20** is correctly predicted to be higher than that of compound **19**. The predictions from model 4 are closer to the observed values than the predictions from model 3, especially for compound **19**, where the prediction is in excellent agreement with the observed value. The rise in transition temperature, observed for compound **23** in DPPA liposomes, is not predicted.

It is remarkable that no elevation in  $T_t$  was observed when compound **23** was added to a DPPC liposome preparation. Figure 5 shows the transition temperatures of both DPPC and DPPA liposomes under the influence of selected analogues. The transition temperatures for compounds **6**, **3**, and **5** are essentially independent of phospholipid headgroup type. This is not the case with compound **23**, which decreases the  $T_t$  of DPPC liposomes by about 4 K to a value of 310.9 K. This observation is much closer to the predicted values of 314 and 298 K, respectively, than the value of 348.8 K, which was observed with DPPA. This supports the validity of our model. Apparently, the interaction of compound **23** with DPPA is governed by molecular events which cannot be adequately modeled by a DPPC simulation system. It would be quite interesting to study the behavior of selected compounds in a DPPA simulation system.

Explanations for the unusual behavior of compound **23** in DPPA can, at best, only be hypothesized. The reason for the increase in  $T_t$  might be because this

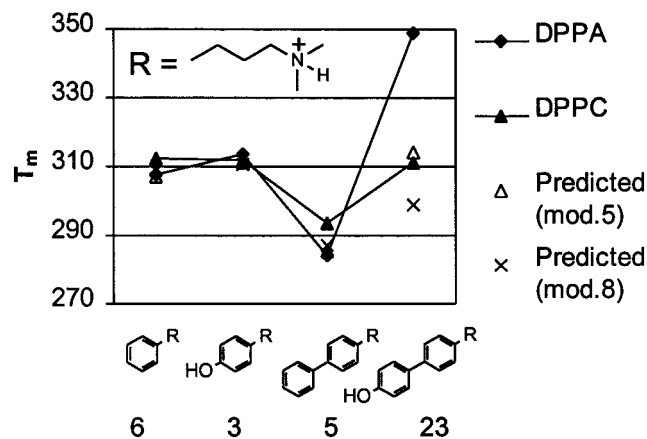


**Figure 5.** Influence of selected compounds on the phase-transition temperatures of DPPA and DPPC liposomes.

**Table 6.** Correlation Coefficients of Average and Minimum Interaction Energies for All Compounds

total	electrostatic	van der Waals	H-bond
0.85	0.94	0.75	0.99

compound adopts a position parallel to the membrane–water interface within the headgroup region, and “cross-links” two or more phospholipids, by means of hydrogen bonds to the phenolic oxygen and, simultaneously, by ionic interactions to the charged amine group. The MDSs support this idea by adopting states in which a solute is aligned parallel to the interface for all phenolic compounds (**3**, **23**, **24**) and the nitro compound (**21**). However, no elevation in  $T_t$  is observed for **24**, **3**, and **21**. Moreover, compound **24**, in fact, is one of the most pronounced  $T_t$ -depressing solutes. A larger specific distance between the amino and the hydroxyl groups of a solute might be necessary to easily permit this “cross-linking” effect. Thus, it would be interesting to study derivatives of compound **23**, e.g., compounds with more than one phenolic hydroxyl group, or the corresponding aromatic amine.

None of the average membrane–solute interaction energies are found as descriptors in the best membrane–interaction QSPR models. Instead, interaction energies at minimum system potential energy are preferred in the best QSPRs. This preference may again be due to incomplete sampling efficiency. A true Boltzmann averaged potential energy distribution over a MDS trajectory is not achieved. Interaction energies at minimum system potential energy may provide the most realistic representation of the most highly populated states of the membrane–solute system. However, all interaction energies at the minimum system potential energy are meaningfully correlated with their average energy counterparts (cf. Table 6).

Finally, a variety of models without any membrane–interaction descriptors emerged from the GFA runs, the best of which (in terms of cross-validated  $r^2$ ) is given as eq 5:

$$T_t = 295.53 - 0.2276*(\text{Jurs-PPSA}_3 - 37.543)^2 + 15.203*(\text{ROG} - 4.674)^2 \quad (5)$$

$$\text{LOF} = 25.652, r^2 = 0.77, xv-r^2 = 0.50, \text{SE} = 4.655, n = 15$$

The statistical fit and significance, particularly in terms of  $xv-r^2$ , of this model are clearly inferior to the two membrane–interaction models given as eqs 3 and 4. Thus, the necessity and significance of intermolecular membrane–interaction descriptors in modeling  $T_t$  are established.

## Conclusions

The main conclusions from this work can be summarized as follows:

Significant QSAR models are developed for  $-\log AC_{50}$ ,  $-\log IC_{50}$ , and  $T_t$  from the pool of trial descriptors generated from intramolecular properties and features **and** from intermolecular membrane–interaction properties generated from the MDS studies.

The sets of descriptors in each of the three QSAR models to respectively describe  $AC_{50}$ ,  $IC_{50}$ , and  $T_t$  are quite different from one another.

The different descriptor sets for each of the  $AC_{50}$ ,  $IC_{50}$ , and  $T_t$  QSAR models suggest that different mechanisms, and/or sites of action, are involved in each of these three properties. The QSAR models also provide a physicochemical basis as to why  $AC_{50}$ ,  $IC_{50}$ , and  $T_t$  measures are not highly correlated among one another.

None of the QSAR descriptors of the  $AC_{50}$  model are derived from explicit membrane interaction MDS modeling. This form of the QSAR suggests, in turn, that the lipid regions of the membrane do not play a major role in the expression of antiarrhythmic activity. Conversely, the QSAR descriptors for  $AC_{50}$  identify specific and/or local physicochemical features of the cationic amphiphilic drugs that are indicative of **specific** ligand–receptor interactions.

The QSAR model for calcium ion replacement does not contain membrane–interaction descriptors characteristic of a compound embedded within the membrane bilayer. However, all of the QSAR descriptors are electrostatic/charge properties in nature and are consistent with electrostatic interactions at the surface of a membrane probably involving the headgroups of the phospholipid.

The depression of the membrane phase-transition temperature,  $T_t$ , is expressed by a QSAR model which contains MDS membrane–interaction descriptors which, in turn, suggests  $T_t$  behavior involves the incorporation of compounds into the hydrocarbon chain region of the membrane bilayer.

The question arises whether the same amount and quality of structure–property information could have been extracted from the “right” set of purely intramolecular solute descriptors. That is, could the membrane–solute MDS modeling have been avoided? We think that the answer is “No”. Some of the membrane–interaction QSAR descriptors are collinear within their own class, but no significant correlation to any intramolecular solute descriptor could be found. This strongly suggests that the membrane–solute descriptors determined by MDS provide significant additional structure–property information that cannot be obtained by any intramolecular measures.

Membrane–interaction descriptors do not appear to be of particular significance in explaining the antiarrhythmic or the calcium-displacing activity of the compounds. This suggests that both endpoints are not primarily



determined by the influence of the compounds on thermodynamic membrane properties. Spatial features, reflected by the grid cell occupancy descriptor in the AC<sub>50</sub> QSAR model, are important for the expression of antiarrhythmic activity and are supported by whole-molecule property descriptors such as surface charge measures. This underscores the importance of penetration and adsorption behavior at some point in the pharmacokinetic–pharmacodynamic chain of the assay system. The MDS sampling protocol employed in this study did not succeed in collecting sufficient structure–property information for certain types of solute–membrane interaction properties. Certainly, the short time scale prevented a reasonable estimation of diffusion coefficients. However, the diffusion behavior is likely to be explained largely by intramolecular descriptors such as log *P* and molecular weight, and the determination of diffusion coefficients by molecular dynamics simulations might be unnecessary.

## Experimental Section

**Chemistry.** Melting points were determined on the Reichert microhotstage and are uncorrected. The 400-MHz proton NMR spectra were recorded on a Bruker AM400 spectrometer, and shifts are expressed in  $\delta$  (ppm) with TMS as internal standard. IR spectra were taken with a Perkin-Elmer FTIR 1600 spectrometer in KBr and are expressed in cm<sup>-1</sup>. Elemental analyses were performed from the Microlaboratory of Ilse Beetz, Kronach, Germany. Analytical results were within 0.4% of the theoretical values. Silicagel thin-layer chromatography was performed on precoated plates Kieselgel 60F<sub>254</sub> (E. Merck, AG, Darmstadt, Germany). Extraction solvents were dried over magnesium sulfate. Starting materials were commercially available (Merck, Aldrich, Fluka), of the best grade, and used without further purification.

**Method A (Scheme 1): General Procedure for the Wittig Reaction of Substituted Benzaldehydes followed by Catalytic Hydrogenation.** To a stirred solution of *N,N*-dimethylaminoethyltriphenylphosphonium bromide (40 mmol) in dry tetrahydrofuran (150 mL) was added an equimolar solution of 1.4 M *n*-butyllithium in *n*-hexane under N<sub>2</sub> at 0 °C. After 30 min a solution of starting benzaldehyde (40 mmol) was added slowly, and then the reaction mixture was stirred overnight at 60 °C. The solution was acidified with 3 N hydrochloric acid (60 mL) and tetrahydrofuran evaporated. After extraction with toluene (twice with 100 mL) the water phase was made alkaline with 3 N sodium hydroxide and extracted with ether (three times with 50 mL). The *N,N*-dimethylcinnamylamine was isolated and converted to the hydrochloride in the usual manner, followed by recrystallization from ethanol/ether.

To a stirred solution or suspension of the propene derivative (30 mmol) in methanol (250 mL) was added 10% palladium-on-carbon (2.0 g). The reaction mixture was held under a positive pressure of hydrogen (300–400 kPa) on a Parr shaker until the theoretical uptake of hydrogen had occurred. The catalyst was removed by filtration, and the filtrate was concentrated to dryness in order to give the crude product. After addition of water (100 mL) the resulting mixture was made alkaline using 3 N sodium hydroxide and subsequently extracted three times with ether (50 mL). The combined organic layer was washed with water and dried, and the hydrochloride was precipitated by addition of ethereal hydrochloric acid, recrystallized twice from ethanol/ether.

**3-(4-Chlorophenyl)-*N,N*-dimethylpropylamine hydrochloride (1):**<sup>41</sup> IR (KBr) 2920, 2490, 1470, 1030, 820 cm<sup>-1</sup>; <sup>1</sup>H NMR (CDCl<sub>3</sub>)  $\delta$  2.17–2.24 (2H, m), 2.73 (2H, t, *J* = 7.37 Hz), 2.79 (6H, d, *J* = 4.91 Hz), 2.93–2.98 (2 H, m), 7.14 (2 H, d, *J* = 8.38 Hz), 7.27 (2 H, d, *J* = 7.96 Hz).

**3-(4-Bromophenyl)-*N,N*-dimethylpropylamine hydrochloride (2):** IR (KBr) 3000, 2510, 1500, 1075, 820 cm<sup>-1</sup>; <sup>1</sup>H

NMR (CDCl<sub>3</sub>)  $\delta$  2.17–2.28 (2H, m), 2.72 (2H, t, *J* = 7.32 Hz), 2.79 (6H, d, *J* = 4.75 Hz), 2.93–3.00 (2 H, m), 7.08 (2 H, d, *J* = 8.30 Hz), 7.43 (2 H, d, *J* = 8.29 Hz).

***N,N*-Dimethyl-3-(4-hydroxyphenyl)propylamine hydrochloride (3):**<sup>42</sup> IR (KBr) 3160, 2980, 2680, 1610, 1010, 810 cm<sup>-1</sup>; <sup>1</sup>H NMR (CDCl<sub>3</sub>)  $\delta$  1.95–2.03 (2H, m), 2.62 (2H, t, *J* = 7.5 Hz), 2.86 (6H, s), 3.07–3.11 (2 H, m), 6.73 (2 H, d, *J* = 8.48 Hz), 7.05 (2 H, d, *J* = 8.40 Hz).

***N,N*-Dimethyl-3-(3-pyridyl)propylamine dihydroperchlorate (4):** IR (KBr) 2940, 1560, 680 cm<sup>-1</sup>; <sup>1</sup>H NMR (CDCl<sub>3</sub>)  $\delta$  2.12–2.20 (2H, m), 2.92 (6H, s), 2.99 (2H, t, *J* = 7.87 Hz), 3.23–3.27 (2 H, m), 8.06 (1 H, dd, *J*<sub>1</sub> = *J*<sub>2</sub> = 5.83 Hz), 8.59 (1 H, d, *J* = 8.13 Hz), 8.73 (1 H, d, *J* = 5.69 Hz), 8.80 (1 H, s).

**Method B (Scheme 2): General Procedure for the Vilsmeier Reaction of Ketones followed by Catalytic Hydrogenation.** To anhydrous *N,N*-dimethylformamide (30.0 mL) was added dropwise phosphorus oxychloride (0.22 mol) at 15–25 °C, and stirring was continued for 1 h at ambient temperature. After addition of ketone (0.02 mol) to the resulting mixture, the temperature was slowly raised to 40 °C. A solution of ketone (0.08 mol) in anhydrous *N,N*-dimethylformamide (10 mL) was added while maintaining the temperature at 70 °C. After 5 h at room temperature methanol (500 mL) was added and then perchloric acid (25 mL, 70%) to form the perchlorate recrystallized from methanol. The 3-chloropropeniminium salts were catalytically hydrogenated using palladium-on-carbon and the resulting amines converted to the hydrochlorides **1** and **4–17** according to method A.

**3-(4-Biphenyl)-*N,N*-dimethylpropylamine hydrochloride (5):** IR (KBr) 2940, 2440, 760 cm<sup>-1</sup>; <sup>1</sup>H NMR (CDCl<sub>3</sub>)  $\delta$  2.22–2.30 (2H, m), 2.78–2.81 (8 H, m), 2.97–3.02 (2 H, m), 7.25–7.59 (9 H, m).

***N,N*-Dimethyl-3-phenylpropylamine hydrochloride (6):**<sup>41</sup> IR (KBr) 2920, 2580, 1480, 700 cm<sup>-1</sup>; <sup>1</sup>H NMR (CDCl<sub>3</sub>)  $\delta$  2.18–2.26 (2H, m), 2.75 (2 H, t, *J* = 2.70 Hz), 2.77 (6 H, d, *J* = 4.90 Hz), 2.94–2.99 (2 H, m), 7.18–7.33 (5 H, m).

***N,N*-Dimethyl-3-(4-methylphenyl)propylamine hydrochloride (7):**<sup>43</sup> IR (KBr) 2950, 2490, 1150, 810 cm<sup>-1</sup>; <sup>1</sup>H NMR (CDCl<sub>3</sub>)  $\delta$  2.15–2.23 (2H, m), 2.32 (3 H, s), 2.70 (2H, t, *J* = 7.23 Hz), 2.77 (6H, d, *J* = 4.87 Hz), 2.92–2.98 (2 H, m), 7.07 (2 H, d, *J* = 8.04 Hz), 7.11 (2 H, d, *J* = 7.35 Hz).

***N,N*-Dimethyl-3-(4-ethylphenyl)propylamine hydrochloride (8):** IR (KBr) 2950, 2520, 1460, 760 cm<sup>-1</sup>; <sup>1</sup>H NMR (CDCl<sub>3</sub>)  $\delta$  1.23 (3H, t, *J* = 7.62), 1.71–2.24 (2H, m), 2.62 (2 H, q, *J* = 7.62 Hz), 2.71 (2 H, t, *J* = 7.24 Hz), 2.77 (6 H, d, *J* = 4.83 Hz), 2.93–2.98 (2 H, m), 7.09 (2 H, d, *J* = 8.05 Hz), 7.14 (2H, d, *J* = 7.89 Hz).

***N,N*-Dimethyl-3-(4-*n*-propylphenyl)propylamine Hydrochloride (9).** Zinc powder (2.5 g) was added to 5 N hydrochloric acid (250 mL) at 5 °C under stirring followed by 2 mL of the Vilsmeier reaction mixture. Alternating, this procedure was continued avoiding too hazardous conditions. After 3 h stirring under cooling the mixture was slowly neutralized with sodium hydroxide and extracted three times with ether (50 mL). The combined organic layer was washed with water and dried, and the hydrochloride was precipitated by addition of ethereal hydrochloric acid, recrystallized twice from acetone/ether: IR (KBr) 2930, 2510, 1450, 1150, 810 cm<sup>-1</sup>; <sup>1</sup>H NMR (CDCl<sub>3</sub>)  $\delta$  0.94 (3 H, t, *J* = 7.34 Hz), 1.62 (2 H, t, *J* = 7.47 Hz), 2.16–2.24 (2H, m), 2.56 (2 H, t, *J* = 7.67 Hz), 2.71 (3 H, t, *J* = 7.25 Hz), 2.77 (6 H, d, *J* = 4.81 Hz), 2.93–2.98 (2 H, m), 7.08 (2 H, d, *J* = 8.19 Hz), 7.12 (2 H, d, *J* = 8.15 Hz).

***N,N*-Dimethyl-3-(4-isopropylphenyl)propylamine hydrochloride (10):** IR (KBr) 2950, 2510, 1460, 1160, 810 cm<sup>-1</sup>; <sup>1</sup>H NMR (CDCl<sub>3</sub>)  $\delta$  1.24 (6 H, d, *J* = 6.95 Hz), 2.16–2.24 (2H, m), 2.72 (2 H, t, *J* = 7.26 Hz), 2.77 (6 H, d, *J* = 4.84 Hz), 2.87 (1 H, dq, *J* = 6.92 Hz), 2.94–2.99 (2 H, m), 7.10 (2 H, d, *J* = 8.04 Hz), 7.16 (2 H, d, *J* = 8.04 Hz).

**3-(4-*tert*-Butylphenyl)-*N,N*-dimethylpropylamine hydrochloride (11):** IR (KBr) 2950, 2580, 1480, 840 cm<sup>-1</sup>; <sup>1</sup>H NMR (CDCl<sub>3</sub>)  $\delta$  1.31 (9 H, s), 2.18–2.24 (2H, m), 2.71 (2 H, t, *J* = 7.28 Hz), 2.78 (6 H, d, *J* = 4.92 Hz), 2.95–3.00 (2 H, m), 7.11 (2 H, d, *J* = 8.25 Hz), 7.33 (2 H, d, *J* = 8.31 Hz).



***N,N*-Dimethyl-3-(4-methoxyphenyl)propylamine hydrochloride (12):**<sup>44</sup> IR (KBr) 2950, 2840, 2530, 1460, 1170, 1120, 820  $\text{cm}^{-1}$ ; <sup>1</sup>H NMR ( $\text{CDCl}_3$ )  $\delta$  2.14–2.22 (2H, m), 2.69 (2H, t,  $J = 7.25$  Hz), 2.77 (6H, d,  $J = 4.92$  Hz), 2.92–2.97 (2H, m), 3.79 (3H, s), 6.85 (2H, d,  $J = 8.64$  Hz), 7.10 (2H, d,  $J = 8.61$  Hz).

**3-(4-Chlorobiphenyl)-*N,N*-dimethylpropylamine hydrochloride (13):** IR (KBr) 2950, 2470, 1110, 820  $\text{cm}^{-1}$ ; <sup>1</sup>H NMR ( $\text{CDCl}_3$ )  $\delta$  2.22 (2H, m), 2.79 (8H, m), 2.97–3.03 (2H, m), 7.26–7.53 (8H, m).

***N,N*-Dimethyl-3-(4'-methoxy-4-biphenyl)propylamine hydrochloride (14):** IR (KBr) 2940, 2830, 2460, 1490, 1240, 1020, 810  $\text{cm}^{-1}$ ; <sup>1</sup>H NMR ( $\text{CDCl}_3$ )  $\delta$  2.23–2.29 (2H, m), 2.76–2.79 (8H, m), 2.96–3.00 (3H, m), 3.85 (3H, s), 6.98 (2H, d,  $J = 8.76$  Hz), 7.23 (2H, d,  $J = 8.07$  Hz), 7.49 (2H, d,  $J = 5.63$  Hz), 7.52 (2H, d,  $J = 6.46$  Hz).

***N,N*-Dimethyl-3-(4'-ethoxy-4-biphenyl)propylamine hydrochloride (15):** IR (KBr) 2960, 2530, 1480, 1250, 1160, 1050, 810  $\text{cm}^{-1}$ ; <sup>1</sup>H NMR ( $\text{CDCl}_3$ )  $\delta$  1.44 (3H, t,  $J = 6.98$  Hz), 2.21–2.29 (2H, m), 2.76–2.78 (8H, m), 2.96–3.01 (2H, m), 4.08 (2H, q,  $J = 6.98$  Hz), 6.97 (2H, d,  $J = 8.75$  Hz), 7.23 (2H, d,  $J = 8.10$  Hz), 7.50 (2H, d,  $J = 8.0$  Hz), 7.51 (2H, d,  $J = 8.0$  Hz).

***N,N*-Dimethyl-3-( $\beta$ -naphthyl)propylamine hydrochloride (16):**<sup>45</sup> IR (KBr) 2940, 2440, 1470, 820  $\text{cm}^{-1}$ ; <sup>1</sup>H NMR ( $\text{CDCl}_3$ )  $\delta$  2.28–2.35 (2H, m), 2.76 (6H, d,  $J = 4.68$  Hz), 2.92 (2H, t,  $J = 7.2$  Hz), 2.96–3.01 (2H, m), 7.27–7.81 (7H, m).

**3-(3-Chloro-4-methoxyphenyl)-*N,N*-dimethylpropylamine hydrochloride (17):** IR (KBr) 2950, 2840, 2600, 1500, 1060, 1020, 810  $\text{cm}^{-1}$ ; <sup>1</sup>H NMR ( $\text{CDCl}_3$ )  $\delta$  2.14–2.22 (2H, m), 2.68 (2H, t,  $J = 7.33$  Hz), 2.77 (6H, d,  $J = 4.9$  Hz), 2.95–2.98 (2H, m), 3.89 (3H, s), 6.87 (1H, d,  $J = 8.39$  Hz), 7.08 (1H, dd,  $J_1 = 2.12$  Hz,  $J_2 = 8.2$  Hz), 7.18 (1H, d,  $J = 2.13$  Hz).

**Method C (Scheme 3): General Procedure for the Preparation of 3,3-Diphenyl-Substituted Propylamines 18 and 19.** 1,1-Diphenyl-substituted ethanol derivatives were prepared by Grignard reactions according to standard procedures. Vilsmeier formylation and catalytical hydrogenation were carried out according to method B.

***N,N*-Dimethyl-3,3-diphenylpropylamine hydrochloride (18):**<sup>46</sup> IR (KBr) 3010, 2340, 1460, 700  $\text{cm}^{-1}$ ; <sup>1</sup>H NMR ( $\text{CDCl}_3$ )  $\delta$  2.61–2.67 (2H, m), 2.76 (6H, d,  $J = 5.15$  Hz), 2.89–2.94 (2H, m), 4.00 (1H, t,  $J = 2.1$  Hz), 7.19–7.33 (10H, m).

**3-(4-Biphenyl)-*N,N*-dimethylpropylamine hydrochloride (19):** IR (KBr) 2910, 2510, 1460, 1150, 750, 680  $\text{cm}^{-1}$ ; <sup>1</sup>H NMR ( $\text{CDCl}_3$ )  $\delta$  2.65–2.71 (2H, m), 2.78 (6H, d,  $J = 4.82$  Hz), 2.93–2.97 (2H, m), 4.05 (2H, t,  $J = 7.87$  Hz), 7.21–7.56 (14H, m).

***N,N*-Dimethyl-2,3-diphenylpropylamine Hydrochloride (20):**<sup>47</sup> **20** was prepared from desoxybenzoin (19.6 g, 0.1 mol) according to method B and the reaction mixture heated for 24 h at 60–70 °C. For the precipitation of the perchlorate, 2-propanol (400 mL) and perchloric acid (25 mL, 70%) were added to the mixture. Catalytic hydrogenation of the resulting iminium salt yielded **20** recrystallized twice from acetone/ether (8.5 g, 86%) as colorless crystals: mp 167–169 °C; IR (KBr) 2950, 2520, 1460, 690  $\text{cm}^{-1}$ ; <sup>1</sup>H NMR ( $\text{CDCl}_3$ )  $\delta$  2.52 (3H, d,  $J = 4.88$  Hz), 2.62 (3H, d,  $J = 4.9$  Hz), 2.95 (1H, q,  $J = 8.1$  Hz), 3.09 (1H, q,  $J = 7.1$  Hz), 3.28–3.35 (1H, m), 3.44 (1H, dt), 3.58–3.65 (1H, m), 7.04–7.33 (10H, m).

***N,N*-Dimethyl-3-(4-nitrophenyl)propylamine Hydrochloride (21):**<sup>42</sup> To a solution of **6** (17 g, 0.1 mol) in concentrated sulfuric acid (40 mL) was added dropwise concentrated nitric acid (6.6 g) at –10 °C. After stirring for 15 h, the mixture was added to crushed ice (100 g) and subsequently alkalinized slowly using sodium hydroxide solution (50%). The mixture was extracted three times with 50 mL of ether. The combined organic layer was washed with water and dried, and the hydrochloride was precipitated by addition of ethereal hydrochloric acid, recrystallized twice from ethanol/ether to give **21** (7.2 g, 28%) as yellow crystals: mp 154 °C; IR (KBr) 2980, 1610, 1490, 760  $\text{cm}^{-1}$ ; <sup>1</sup>H NMR ( $\text{CDCl}_3$ )  $\delta$  2.27–2.31 (2H, m),

2.82 (6H, d,  $J = 3.35$  Hz), 2.90 (2H, t,  $J = 7.48$  Hz), 2.98–3.05 (2H, m), 7.41 (2H, d,  $J = 9.45$  Hz), 8.81 (2H, d,  $J = 8.53$  Hz).

**3-Phenyl-*N,N,N*-trimethylpropylammonium Iodide (22):**<sup>48</sup> A mixture of **6** (6.75 g, 50 mmol), methyl iodide (43.2 g, 0.3 mol), and potassium carbonate (12 g) in water (80 mL) was refluxed for 7 h. Excess of methyl iodide was evaporated and the residue extracted three times with 50 mL of dichloromethane. The combined organic layer was dried and evaporated. The residue was recrystallized from ethanol/ether to give **22** (13.4 g, 88%) as colorless crystals: mp 175 °C (173 °C);<sup>28</sup> IR (KBr) 3000, 1470, 720  $\text{cm}^{-1}$ ; <sup>1</sup>H NMR ( $\text{CD}_3\text{OD}$ )  $\delta$  2.09–2.17 (2H, m), 2.72 (2H, t,  $J = 7.57$  Hz), 3.13 (9H, s), 3.35–3.40 (2H, m), 7.19–7.32 (5H, m).

***N,N*-Dimethyl-3-(4'-hydroxy-4-biphenyl)propylamine Hydrochloride (23):** A mixture of the methyl ether **14** (4 g, 13 mmol) in concentrated hydrobromic acid (40 mL) was refluxed for 2 h. After cooling, to the mixture was added slowly water (100 mL), and the resulting mixture was alkalinized with concentrated ammonia to give pH 9. The resulting solution was extracted three times with 75 mL of ether. The combined organic layer was washed twice with water and dried, and 120 mL of the solvent was evaporated. After addition of ethereal hydrochloric acid the crude product was recrystallized from ethanol/ether to give **23** as colorless crystals: IR (KBr) 3140, 2940, 2680, 1490, 1210, 800  $\text{cm}^{-1}$ ; <sup>1</sup>H NMR ( $\text{CD}_3\text{OD}$ )  $\delta$  2.02–2.10 (2H, m), 2.74 (2H, t,  $J = 7.53$  Hz), 2.88 (6H, s), 3.12–3.31 (2H, m), 6.84 (2H, d,  $J = 8.62$  Hz), 7.27 (2H, d,  $J = 8.13$  Hz), 7.42 (2H, d,  $J = 8.63$  Hz), 7.49 (2H, d,  $J = 8.19$  Hz).

**3-(3-Chloro-4-hydroxyphenyl)-*N,N*-dimethylpropylamine Hydrochloride (24):** obtained following a procedure similar to that for compound **23**; IR (KBr) 3100, 2950, 1470, 1280, 1160, 1050, 810  $\text{cm}^{-1}$ ; <sup>1</sup>H NMR ( $\text{CD}_3\text{OD}$ )  $\delta$  1.95–2.03 (2H, m), 2.61 (2H, t,  $J = 7.57$  Hz), 2.86 (6H, s), 3.08–3.12 (2H, m), 6.85 (1H, d,  $J = 8.25$  Hz), 7.01 (1H, dd,  $J_1 = 2.03$  Hz,  $J_2 = 8.2$  Hz), 7.2 (1H, d,  $J = 1.97$  Hz).

**3-(4'-Methoxy-4-biphenyl)-*N,N,N*-trimethylpropylammonium Chloride (25):** Compound **25** was obtained following a procedure similar to that for compound **22**. The resulting iodide (2.4 g, 6.0 mmol) was dissolved in methanol (40 mL), and the solution was saturated with gaseous hydrochloric acid and heated at 100 °C for 1 h in an open round-bottom flask. The residue was recrystallized from ethanol/ether to give **25** (1.8 g, 94%) as colorless crystals: mp 137 °C; IR (KBr) 2940, 2830, 1490, 1030, 800  $\text{cm}^{-1}$ ; <sup>1</sup>H NMR ( $\text{CD}_3\text{OD}$ )  $\delta$  2.12–2.20 (2H, m), 2.75 (2H, t,  $J = 7.45$  Hz), 3.13 (9H, s), 3.36–3.39 (2H, m), 3.82 (3H, s), 6.99 (2H, d,  $J = 8.77$  Hz), 7.31 (2H, d,  $J = 8.05$  Hz), 7.51 (2H, d,  $J = 8.40$  Hz), 7.52 (2H, d,  $J = 8.00$  Hz).

**3-*N,N*-Dimethyl-3-(4-aminophenyl)propylamine Hydrochloride (26):**<sup>42</sup> To a stirred solution of **21** (2.4 g, 10 mmol) in methanol (100 mL) was added 10% palladium-on-carbon (1.0 g). The reaction mixture was held under a positive pressure of hydrogen (300–400 kPa) on a Parr shaker until the theoretical uptake of hydrogen had occurred. The catalyst was removed by filtration, and the filtrate was concentrated to dryness. To the residue was added water (100 mL); the resulting mixture was made alkaline using 3 N sodium hydroxide and subsequently extracted three times with ether (50 mL). The combined organic layer was washed with water and dried, and the hydrochloride was precipitated by addition of ethereal hydrochloric acid, recrystallized twice from ethanol/ether to give **22** (2.4 g, 80%) as colorless crystals: mp 250 °C dec; IR (KBr) 2775, 2520, 1550, 1450, 1150, 810  $\text{cm}^{-1}$ ; <sup>1</sup>H NMR ( $\text{CD}_3\text{OD}$ )  $\delta$  2.03–2.11 (2H, m), 2.77 (2H, t,  $J = 7.91$  Hz), 2.89 (6H, s), 3.15–3.19 (2H, m), 7.36 (2H, d,  $J = 8.42$  Hz), 7.46 (2H, d,  $J = 8.36$  Hz).

**QSAR Analysis: Computational Details. 1. dp (change in membrane density upon uptake of the solute).** The Connolly volume for the lowest potential energy state of the reference monolayer model (without any solute) was determined. A probe with a radius of 1.4 Å was employed. The procedure was repeated for the lowest potential energy state of each monolayer–solute system and the corresponding

change in density was calculated as

$$dp = \frac{M_{(\text{mem}+\text{sol})}}{V_{(\text{mem}+\text{sol})}} - \frac{M_{\text{mem}}}{V_{\text{mem}}} \quad (1)$$

where  $M_{\text{mem}}$  is the mass of the model monolayer without the solute,  $M_{(\text{mem}+\text{sol})}$  is the mass of the monolayer-solute system, and  $V_{(\text{mem}+\text{sol})}$  and  $V_{\text{mem}}$  are the respective volumes.

**2.  $D$  (solute diffusion coefficient).** The mean-square displacement method was used to calculate diffusion coefficients. For each trajectory frame in the MDS trajectory, the average movement  $\Delta d_i$  of a solute molecule, relative to the previous frame, was determined. The mean square distance is defined as

$$\bar{\chi}^2 = \frac{\sum_{i=1}^n \Delta d_i^2}{t} \quad (2)$$

where  $t$  is the total simulation time and  $n$  denotes the number of MDS frames. Using the Einstein<sup>49</sup> diffusion equation, the diffusion coefficient  $D$  can be calculated as

$$D = \frac{\bar{\chi}^2}{2t} \quad (3)$$

**3.  $\langle d \rangle$  (average depth of a solute in the membrane).** For each trajectory frame, the distances between the aromatic carbon bearing the aminopropyl side chain of the solute and five adjacent phospholipid phosphorus atoms were determined. The trajectory average distance between the aromatic carbon and a single phosphorus atom was computed as

$$\langle d_{(\text{single})} \rangle = \sum_{i=1}^n p_i d_i \quad (4)$$

where  $p_i$  is the thermodynamic probability of the  $i$ th state (see below). The average of all five carbon-phosphorus trajectory average distances was used as the average depth descriptor,  $\langle d \rangle$ . The thermodynamic probability of each state in the MDS trajectory can be calculated as

$$p_i = \frac{e^{(-E_i/RT)}}{Q} \quad (5)$$

where  $E_i$  denotes the potential energy of the  $i$ th state and  $Q$  is the partition function, approximated from the MDS trajectory total potential energies:

$$Q = \sum_{i=1}^n e^{(-E_i/RT)} \quad (6)$$

**4.  $dS$  (change in entropy of the membrane system upon uptake of a solute).** The thermodynamic probability of each state of the MDS trajectory was calculated for the reference monolayer system (without solute) and the solute-containing system. The change in entropy upon uptake of a solute was computed as

$$dS = -\frac{R}{m} \left[ \sum_{i=1}^n (p_{i(\text{mem}+\text{sol})} \ln p_{i(\text{mem}+\text{sol})} - p_{i(\text{mem})} \ln p_{i(\text{mem})}) \right] \quad (7)$$

where  $m$  denotes the number of phospholipids in the system, and  $p_{i(*)}$  are the thermodynamic probabilities of the respective systems for the  $i$ th state.

Additional membrane-interaction descriptors, namely the change in bulk modulus, the cohesive energy density, the change in free volume, and the free energy of transfer from water to membrane, were calculated for several compounds.

However, these computational experiments revealed that either the method of calculation could not be meaningfully applied to the highly disordered membrane system (bulk modulus) or the variances in the measures were not large enough to promise any information in QSPR model construction. (The AM1 charges of the training set molecules and the DPPC molecules are available from the principal author, C.D.P.K.)

**Acknowledgment.** This work was supported in part (UIC staff) by the Procter & Gamble Co. Resources of the Laboratory of Molecular Modeling and Design were used to perform the modeling part of this study. The stimulating discussions with Prof. U. Holzgrabe at the University of Bonn are gratefully acknowledged. We greatly appreciate computer support from Dr. J. Triebs of 8810M55 Programming GmbH. C.K. acknowledges financial support from the Konrad Adenauer-Stiftung.

## References

- (1) Girke, S.; Mohr, K.; Schrape, S. Comparison Between the Activities of Cationic Amphiphilic Drugs to Affect Phospholipid-Membranes and to Depress Cardiac Function. *Biochem. Pharmacol.* **1989**, *38*, 2487-2496.
- (2) Lüllmann, H.; Mohr, K. Drug Phospholipid Interactions. In *Metabolism of Xenobiotics*; Gorrod, J. W., Oelschläger, H., Caldwell, J., Eds.; Taylor & Francis: London, 1988.
- (3) Seydel, J. K.; et al. QSAR and Multivariate Data Analysis of Amphiphilic Benzylamines and their Interaction with Various Phospholipids Determined By Different Methods. *QSAR* **1989**, *8*, 266-278.
- (4) Lüllmann, H.; Plösch, H.; Ziegler, A. Ca<sup>2+</sup> Replacement by Cationic Amphiphilic Drugs from Lipid Monolayers. *Biochem. Pharmacol.* **1980**, *29*, 2969-2974.
- (5) Borchardt, K.; Heber, D.; Klingmüller, M.; Mohr, K.; Müller, B. The Ability of Cationic Amphiphilic Compounds to Depress the Transition Temperature of Dipalmitoylphosphatidic Acid Liposomes Depends on the Spatial Arrangement of the Lipophilic Moiety. *Biochem. Pharmacol.* **1991**, *42* (Suppl.), S61-S65.
- (6) Hanpft, R.; Mohr, K. Influence of Cationic Amphiphilic Drugs on the Phase-Transition Temperature of Phospholipids with Different Polar Headgroups. *Biochim. Biophys. Acta* **1985**, *814*, 156-162.
- (7) Klein, C.; Hopfinger, A. J. Pharmacological activity and membrane interactions of antiarrhythmics: 4D-QSAR/QSPR analysis. *Pharmacol. Res.* **1998**, *15*, 303-311.
- (8) Bassolino, D.; Alper, T. R. Stouch Drug Membrane Interactions Studied by Molecular Dynamics Simulation: Size Dependence of Diffusion. *Drug Des. Discovery* **1996**, *13*, 135-141.
- (9) Jin, B. Q.; Hopfinger, A. J. Characterization of Lipid Membrane Dynamics by Simulation: 3. Probing Molecular Transport Across the Phospholipid Bilayer. *Pharmacol. Res.* **1996**, *12*, 1786-1794.
- (10) Tieleman, D. P.; Marrink, S. J.; Berendsen, H. J. C. A computer perspective of membranes: molecular dynamics studies of lipid bilayer systems. *Biochim. Biophys. Acta* **1997**, *1331*, 235-270.
- (11) Hopfinger, A. J.; Wang, S.; Tokarski, J. S.; Jin, B.; Albuquerque, M.; Madhav, P.; Duraiswami, C. Construction of 3D-QSAR models using the 4D-QSAR analysis formalism. *J. Am. Chem. Soc.* **1997**, *119*, 10509-10524.
- (12) Kuroda, Y.; Fujiwara, Y. Locations and Dynamical Perturbations for Lipids of Cationic Forms of Procaine, Tetracaine, and Dibucaine in Small Unilamellar Phosphatidylcholine Vesicles As Studied by Nuclear Overhauser Effects in 1H Nuclear Magnetic Resonance Spectroscopy. *Biochim. Biophys. Acta* **1987**, *903*, 395-410.
- (13) Mannich, C.; Heilner, G. Syntheses of  $\beta$ -Ketobases from Acetophenone, Formaldehyde, and Amine Salts. *Ber. Dtsch. Chem. Ges.* **1922**, *55*, 356-365.
- (14) Mannich, C.; Chang, F. T. About the Synthesis of Organic Bases with Threefold Binding. *Chem. Ber.* **1933**, *66*, 418-420.
- (15) Yamada, S.; Kikugawa, Y.; Ikegami, S. Reduction of Acid Amides to Amines with Sodium Borohydride. *Chem. Pharm. Bull.* **1965**, *13*, 394-402.
- (16) Ison, R. R.; Hassan, M. M. A. Clemmensen Reduction of Mannich Bases: Potential Ganglionic and Nicotinic Agents. *J. Pharm. Sci.* **1973**, *62*, 1388-1390.
- (17) Stütz, A.; Georgopoulos, A.; Granitzer, W.; Petranyi, G.; Berney, D. Synthesis and Structure-Activity Relationships of Naftifine-Related Allylamine Antimycotics. *J. Med. Chem.* **1986**, *29*, 112-125.
- (18) Kindler, K.; Hedemann, B.; Schärfe, E. Studies on the Mechanism of Chemical Reactions. X. Phenyl- and Cyclohexylalkylamines by Hydrogenation. *Justus Liebigs Ann. Chem.* **1948**, *560*, 215-221.

- (19) Marxer, A.; Leutert, T. The Aminoalkylation of Carbonyl Compounds with Aid of the Wittig-Reaction. *Helv. Chim. Acta* **1978**, *61*, 1708–1716.
- (20) Zemlicka, J.; Arnold, Z. Synthetic Reactions of Dimethylformamide. XI. Polyformylation of Ketones of Other Types and the Problem of the Reaction Course. *Collect. Czech. Chem. Commun.* **1961**, *26*, 2852–2864.
- (21) Liebscher, J.; Hartmann, H. 3-Chloro-2-propeniminium Salts (Vinylous Amide Chloride) as Versatile Synthons in Organic Chemistry. *Synthesis* **1979**, *10*, 241–264.
- (22) Fischer, G. W. <sup>1</sup>H NMR-Spectroscopic Studies on 3-Chloro-2-propeniminium Salts. *J. Prakt. Chem.* **1989**, *311*, 111–114.
- (23) Pearlstein, R. A. *CHEMLAB-II Users Guide*; CHEMLAB Inc., 1780 Wilson Dr, Lake Forest, IL 60045; 1988.
- (24) HyperChem, Release 4.5 for MS Windows; Hypercube Inc., Waterloo, Ontario, Canada; 1995.
- (25) Hauser, H.; Pascher, I.; Pearson, R. H.; Sundell, S. Preferred conformation and molecular packing of phosphatidylethanolamine and phosphatidylcholine. *Biochim. Biophys. Acta* **1981**, *650*, 21–51.
- (26) Stewart, J. J. P. Mopac 6.0 Release Notes; Frank J. Seiler Research Laboratory, United States Air Force Academy; 1990.
- (27) Nagle, J. F. Area/lipid of bilayers from NMR. *Biophys. J.* **1993**, *64*, 1476–1481.
- (28) Jin, B. Q.; Hopfinger, A. J. Characterization of Lipid Membrane Dynamics by Simulation: 1. Torsion Angle Motions of the Linear Chains. *Biopolymers* **1997**, *41*, 37–50.
- (29) Jin, B. Q.; Hopfinger, A. J. Characterization of Lipid Membrane Dynamics by Simulation: 2. Quantitative Representation of Lipid Fluidity. *Comput. Polym. Sci.* **1996**, *6*, 95–101.
- (30) Doherty, D. C. *Molsim Version 3.0 User Guide*; The Chem21 Group, Inc., Lake Forest, IL 60045; 1994.
- (31) Berendsen, H. J. C.; Postma, J. P. M.; van Gunsteren, W. F.; DiNola, A.; Haak, J. R. Molecular dynamics with coupling to an external bath. *J. Chem. Phys.* **1984**, *81*, 3684–3590.
- (32) *Cerius2, V.3.0 User Guide*; Molecular Simulations Inc., San Diego, CA; 1997.
- (33) Stanton, D. T.; Jurs, P. C. Development and Use of Charged Partial Surface Area Structural Descriptors in Computer-Assisted Quantitative Structure–Property Relationship Studies. *Anal. Chem.* **1990**, *62*, 2323–2329.
- (34) Rogers, D. Wolf 6.2 GFA Program; Molecular Simulations Inc.: 1994.
- (35) Glen, W. G.; Dunn, W. J., III; Scott, D. R. Principal Components Analysis and Partial Least Squares Regression. *Tetrahedron Comput. Methodol.* **1989**, *2*, 349–376.
- (36) Rogers, D.; Hopfinger, A. J. Application of Genetic Function Approximation to Quantitative Structure–Activity Relationships and Quantitative Structure–Property Relationships. *J. Chem. Inf. Comput. Sci.* **1994**, *34*, 854.
- (37) Friedman, J. *Multivariate Adaptive Regression Splines*; Technical Report No. 102; Laboratory for Computational Statistics, Department of Statistics, Stanford University; 1988.
- (38) Gasteiger, J.; Marsili, M. Iterative partial equalization of orbital electronegativity – a rapid access to atomic charges. *Tetrahedron* **1998**, *36*, 3219–3228.
- (39) Hopfinger, A. J. *Conformational Properties of Macromolecules*; Academic Press: New York, London, 1973.
- (40) Rauls, D. O.; Baker, J. K. Relationship of nonspecific antiarrhythmic and negative inotropic activity with physicochemical parameters of propranolol analogues. *J. Med. Chem.* **1979**, *22*, 81–86.
- (41) McMahon, R. E. Demethylation Studies I. The Effect of Chemical Structure and Lipid Solubility. *J. Med. Pharm. Chem.* **1961**, *4*, 67–74.
- (42) van Braun, J.; Deutsch, H. Syntheses in the Fatty Aromatic Series (VII. Phenolic Bases). *Ber. Dtsch. Chem. Ges.* **1912**, *45*, 2504–2522.
- (43) Brown, B. G.; Hey, P. Choline Phenyl Ethers as Inhibitors of Amine Oxidase. *Br. J. Pharmacol.* **1956**, *11*, 58–64.
- (44) Kindler, K.; Burghard, F. Reactions of Aromatic Carbaldehydes to  $\beta$ -Arylethylamines. *Arch. Pharm. (Berlin)* **1927**, *265*, 396–397.
- (45) Chandross, E. A.; Thomas, H. T. Intramolecular Exciplex Formation in Naphthylalkylamines. *Chem. Phys. Lett.* **1971**, *9*, 393–397.
- (46) Ruddy, A. W. Antispasmodics II Substituted  $\gamma$ -( $\beta$ -Aminoethyl)-phenylacetoneitriles and 3-Phenylpropylamines. *J. Am. Chem. Soc.* **1951**, *73*, 4096–4098.
- (47) Mattocks, A. M.; Hutchison, O. S. Sympathomimetics: 2,3-Diphenylpropylamines. *J. Am. Chem. Soc.* **1948**, *70*, 3516–3517.
- (48) Fry, J. L.; Silverman, S. B.; Orfanopoulos, M. Reduction of Ketones to Hydrocarbons with Triethylsilane: *m*-Nitroethylbenzene. *Org. Synth.* **1981**, *60*, 108–112.
- (49) Einstein, A. *Investigations on the theory of the brownian movement*; Methuen & Co. Ltd.: London, 1926.

JM980694A